CHALMERS

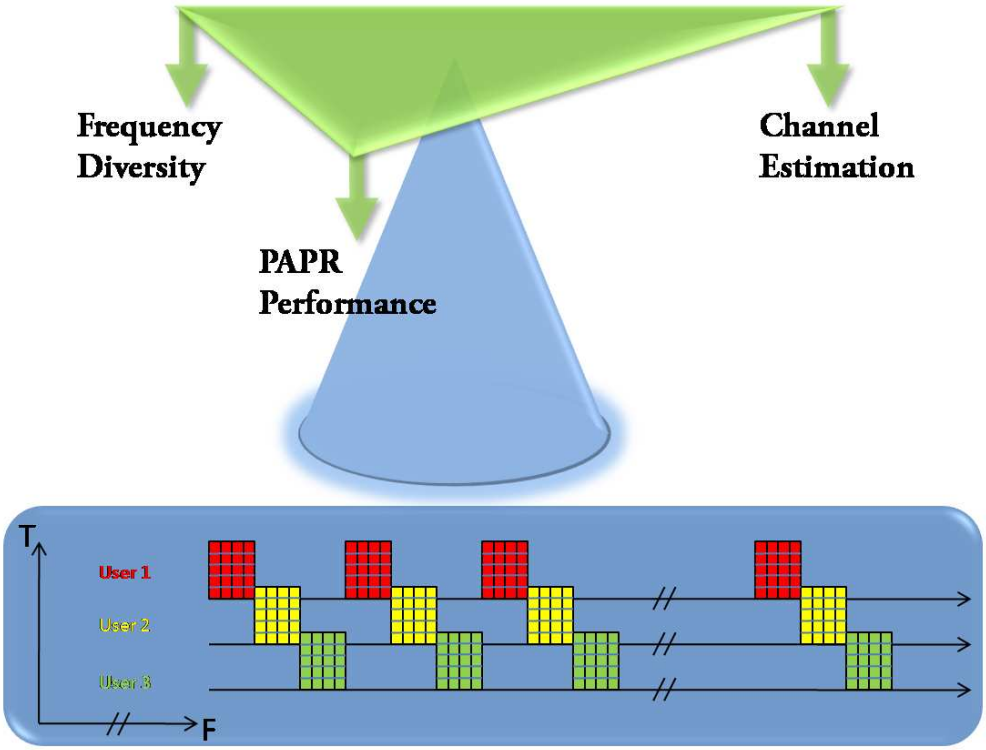

Uplink Multiple Access For IMT-Advanced

Leela Srikar Muppirisetty

Johnny Karout

Department of Signals and Systems
CHALMERS UNIVERSITY OF TECHNOLOGY
Göteborg, Sweden

EX032/2009

Authors contributed equally to this work.

Uplink Multiple Access For IMT-Advanced

Thesis for the degree of Master of Science

Front cover: The top figure shows the trade-off between the parameters, and the lower figure shows the architecture of Block-Interleaved Frequency Division Multiple Access.

ABSTRACT

The wireless communication industry has always been under tremendous improvements in the past few decades, but will the needs for improvement reach an end? Not at all! The challenge for the future wireless systems is the ability to operate in widely different deployment scenarios supporting different traffic rates. As part of the International Telecommunication Union Radiocommunication Sector (ITU-R) International Mobile Telecommunication (IMT) Advanced capable Wireless World Initiative New Radio (WINNER) system concept, a diversity based multiple access scheme for robust uplink transmission denoted as Block Interleaved Frequency Division Multiple Access (B-IFDMA) was proposed to be used in scenarios where transmit channel state information is not readily available due to the imposed overhead, e.g. as with high speed or low data rate and for short control packets.

With its dispersed allocation of multiple blocks with equidistant spacing in frequency, where each block consists of a few consecutive subcarriers in a few consecutive Orthogonal Frequency Division Multiple Access (OFDMA) symbols (Svensson *et al.* 2007), this scheme obtains its robustness and takes advantage of the wireless channel characteristics.

Moreover, the dimension of the blocks allocated enables a tunable degree of frequency diversity and low allocation signaling overhead. In addition, it allows the high power amplifiers (HPA) in the uplink to operate at higher efficiencies because of the use of a Discrete Fourier Transform (DFT) precoding step. In addition, the flexibility of slot allocations enables robust and efficient transmission even for small packets while improving the battery life in user terminals.

In this thesis, end-to-end analysis of B-IFDMA and the other candidate multiple access DFT-precoded techniques Interleaved FDMA (IFDMA), Localized FDMA (LFDMA), together with the non DFT-precoded Block Equidistant FDMA (B-EFDMA) was carried under different deployment scenarios. This was followed by optimal parameter extraction since the results were highly dependent on all the modules involved ranging from the equalization schemes, modulation techniques, channel coding methods, to the channel estimation performance at the receiver.

With perfect channel state information at the receiver, Minimum Mean Square Error (MMSE) equalization and, no pulse shaping, IFDMA provides high frequency diversity and low peak-to-average power ratio (PAPR), compared to LFDMA. However, in more realistic scenarios, LFDMA has a much better channel estimation performance at the receiver, the difference in PAPR after pulse shaping is rather small, and combined with frequency hopping rather good frequency diversity can be obtained with a penalty on an increased packet transmission delay. The B-IFDMA scheme aims to provide a trade-off between the strengths of IFDMA and that of LFDMA for very wideband scenarios and in situations where the delay requirements are stringent, e.g. due to multi-hop transmission. On the other hand, the non DFT-precoded

scheme B-EFDMA collects as much frequency diversity as in B-IFDMA with very close bit error rate performance, but suffers from high back-off requirements on the HPA at the transmitter (user terminal). Despite its worst PAPR, it performs the best in the presence of Zero Forcing (ZF) equalization. Lastly, all these schemes were beneficial in collecting diversity even in the presence of robust channel codes.

Keywords: IMT-Advanced, Multiple Access, DFT-precoding, Frequency diversity, B-IFDMA, IFDMA, LFDMA, B-EFDMA, PAPR, Channel Estimation.

ACKNOWLEDGEMENTS

Now it's time to thank each and every person whom without them, this work wouldn't have been possible. Assist. Professor Tommy Svensson, you are not just a professional supervisor, but an excellent researcher with broad vision too. Indeed, we have made the right choice! Million thanks for agreeing on proposing such an interesting and challenging thesis to us despite your extremely busy schedule. Our deepest gratitude to Assoc. Professor Thomas Eriksson for being our examiner, Professor Erik Ström for his excellent Wireless Communications course notes and projects which were very useful in this thesis. Special thanks to Assoc. Professor Erik Agrell for his sharp and clear guidance regarding the channel coding issues that we faced. We are also grateful to the Communication System group members including Dr. Andreas Wolfgang, Nima Seifi, Alex Alvarado, Kasra Haghighi, Parham Hashemzadeh, Arash Tahmasebi Toyserkani, Panagiota Lioliou, and Guillermo Garcia for their valuable help and suggestions in their area of expertise. Not to forget the people behind the C3SE cluster to whom we owe a thanks for their technical support.

Johnny:

"From the people who were a good source of advice, to those who made me smile, and not to forget those who were just there when needed; you all deserve the credit to being mentioned as contributors to this project and to its success. Randa, besides being a sister and a friend too, you were my main source of motivation pushing me always to the best. It is really hard to thank such a person like you! Elias, your hospitality and generosity meant a lot and I assure you that what you did will never be forgotten. Jonathan, my seven years old nephew who got so involved in the simulation process of the results included in this thesis, has matured a lot in the past two years, surprised me with his mathematical knowledge and analysis skills; I am really happy. Jennifer, you are the cutest niece and I am lucky to have you. The way you think, and the way you talk contradicts with the fact that you are just four years old. You guys made me have a pleasant stay in Sweden and you taught me a lot!!

Mum, now it's time to thank you although these words are just not enough. Despite the distance factor, your wisdom, advice, and continuous support influenced my everyday decisions and were a drive to make me what I am now. I hoped that Dad was still alive just to tell him that the motivation he used to give me, the words he used to say, and the good human values he used to cherish are still alive and are invaluable to me. Brothers, although each had and still has his own way of support, I owe you all a big thank you. Roger, you make the impossible possible. Simon, you always manage to put a smile on people's face. Peter, you know how to take care of the people surrounding you. I am really lucky to have you all! There are also two special persons whom I didn't have the chance to thank before; Amal Badr, with my deepest gratitude, thank you for the inspiration, advice, and the guidance

that you gave me; Assist. Professor Iyad Ouaiss, your advice was and will always be appreciated and of a high value to me, thank you for everything. Lastly, I would like to mention that it was a very nice experience to work with Srikar, who had a completely different schedule which made arranging meetings a tough task, but we made it! You were a colleague before we started this work together but now you are a good friend too!! I wish you all the best in your future plans."

Srikar:

"I am very very thankful to my brother Chakrapani and his wife Swathi. Brother, you are always my main source of inspiration and motivation. Without your constant guidance and help, I wouldn't be where I am now. You are the best teacher I have gotten until now, and a role model too. I really learned a lot from you during these years, especially aiming high, achieving it with hardwork, and never giving up attitude regardless of the harsh hurdles that might come across. I am very lucky to have a brother like you. My deepest gratitude to my Dad and Mom who always supported and encouraged me in whatever I am interested. I am really indebted to them a lot, and I hope that I am now what they wanted me to be.

Thank you Ranjit for having you as the best flatmate possible, it was really fun staying with you through out this period. Thanks for the wonderful discussions and chats on various topics together with you and Raghu (Regenerative Repeater, that's what we call him). Thanks a lot to Prasad, Bhanu, Harsha and Prashant for having wonderful Badminton games and swimming sessions during weekends, you guys made me have an unforgettable birthday in Sweden. Also it was a wonderful experience to work with you Johnny, challenging each other for the perfection of our work. Having met you, I was introduced to a new country 'Lebanon', with new culture, and interesting people. I hope that we meet again sometime, someday , either in India or in Lebanon, the country which I now know a lot about. I wish you all the best for your Ph.D. studies, and I hope you will be a successful researcher. I would also like to thank Chalmers and Sweden for giving me the opportunity to pursue my Master's degree. Finally thanks to everyone who made me have a nice stay in Sweden."

CONTENTS

List of Figures

List of Tables

NOTATION

AWGN	Additive White Gaussian Noise
B-EFDMA	Block Equidistant Frequency Division Multiple Access
BER	Bit Error Rate
B-IFDMA	Block Interleaved Frequency Division Multiple Access
CCDF	Complementary Cumulative Distribution Function
CDMA	Code Division Multiple Access
Conv	With Convolutional Coding
CSIR	Channel State Information at the Receiver
DFT	Discrete Fourier Transform
EGPRS	Enhanced General Packet Radio Service
FDM/FDMA	Frequency Division Multiplexing/Multiple Access
GPRS	General Packet Radio Service
GSM	Global Systems for Mobile Communications
HPA	High Power Amplifiers
HSPA	High Speed Packet Access
ICI	Inter-carrier Interference
IFDMA	Interleaved Frequency Division Multiple Access
IMT	International Mobile Telecommunications
Intv	With Interleaver
IP	Internet Protocol
ISI	Inter-symbol Interference
ITU-R	International Telecommunication Union Radiocommunication Sector
L	Block Size
LFDMA	Localized Frequency Division Multiple Access
LOS	Line Of Sight
LTE	Long Term Evolution
Mbps	Mega Bit Per Second
MMSE	Minimum Mean Square Error Equalizer
NonIntv	Without Interleaver
OFDM/OFDMA	Orthogonal Frequency Division Multiplexing/Multiple Access
PAPR	Peak-To-Average Power Ratio
PDF	Probability Density Funtion
PS	Pulse Shaping
SC-FDE	Single Carrier with Frequency Domain Equalization
SC-FDMA	Single Carrier Frequency Division Multiple Access
SMS	Short Message Service
TDMA	Time Division Multiple Access
UMTS	Universal Mobile Telecommunications System
W-CDMA	Wideband Code Division Multiple Access
WINNER	Wireless World Initiative New Radio
ZF	Zero Forcing Equalizer

1 INTRODUCTION

Competition is the name of the game, and the ability to achieve high data rates and provide better services, determines the winner. This was the theme governing the wireless communication industry in the past few decades. Will it change? Not at all!!

Starting with the first generation (1G) systems that was first deployed in Norway in 1981, analog communications was governing, and the voice transmission was the only service that was supported. Although it was a breakthrough, the urge for improvement arose. There was a need to achieve a higher network capacity, higher speed and improved power efficiency while reducing the overall cost (Goldsmith 2005).

Therefore, second generation (2G) systems emerged satisfying the required needs. The most popular 2G technologies is known as Global Systems for Mobile Communications (GSM) which was developed in Europe. It uses Frequency Division Multiple Access (FDMA) to split the available frequency spectrum, and Time Division Multiple Access (TDMA) to divide each frequency carrier into eight time slots allowing eight simultaneous users to utilize the same frequency. Meanwhile, Code Division Multiple Access (CDMA) technology was developed in North America which uses spread spectrum and special coding techniques to allow users having uniquely assigned codes to be multiplexed over the same channel (V. Pereira 2004). 2G systems were able to handle low data rate services such as fax and Short Message Service (SMS). Even such capabilities weren't enough to catch up with the data intensive applications and with the rise of the internet. Therefore, the 2.5G systems added packet data capability to GSM networks by introducing General Packet Radio Service (GPRS) and Enhanced GPRS (EGPRS), thus enhancing the data capacity of GSM. This adds Internet Protocol (IP) support to the existing GSM network (V. Pereira 2004).

As mobile broadband internet access has become a necessity besides the bandwidth demanding wide spread multimedia applications, something was supposed to be done to support such needs. Therefore third generation systems (3G), known as Universal mobile telecommunications system (UMTS), which were the vision to reach International Mobile Telecommunications (IMT) 2000 standard, came into sight to comply with the high data rate requirements, and higher network capacity. UMTS uses the Wideband Code Division Multiple Access (W-CDMA) radio technology which is characterized by utilizing a wider band than CDMA. This was followed by High Speed Packet Access (HSPA) allowing data rates up to 20 Mega bit per second (Mbps) (E. Dahlman 2008).

With this high data rate provided, 3G seems to satisfy what users want. But is it enough? Of course not! The internet is unleashing more bandwidth intensive applications, shaping the way we communicate, providing a better user experience

and influencing our everyday life. So, new technologies started emerging to reach IMT-Advanced specifications ranging from spectral efficiency to reduced latency, and cutting down overall system cost thus fulfilling the current demands. Long Term Evolution (LTE) is the first step into the fourth generation systems (4G) world providing data rate up to 300 Mbps. This technology had to replace the air interfaces used in previous technologies in order to meet IMT-Advanced objectives (Rumney 2008). As a result, the new radio access network used in LTE is now based on Orthogonal Frequency Division Multiplexing (OFDM) air interface which will be explored in chapter 3.

The remainder of this chapter is to introduce unfamiliar reader to the basics of digital communications system which will serve as a foundation for a better understanding of the remaining material and our contribution to the field. Interested readers will be referred throughout the chapters to classic texts for the concepts involved in this dissertation. This chapter will be concluded by cementing the framework of the whole thesis work.

1.1 Digital Communication Systems

A communication system in general consists of a transmitter, a channel, and a receiver as shown in the figure 1.1.

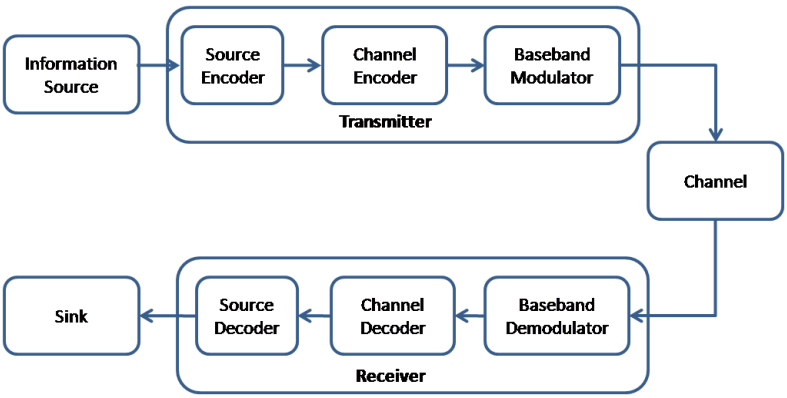

Figure 1.1. Shannon's Digital Communication Model.

Digital communication systems in particular are a subclass where the information to be sent is represented by bits. The information source produces the message to be sent; the transmitter encodes the message to signals and transmits it over the communication channel. The channel alters the transmitted signals by applying different types of distortions/imperfections. The receiver tries to decode the received distorted signals to recover the message that has been transmitted. Another challenge is to let different users communicate over the same channel medium. This issue can be tackled using the different multiple access schemes.

1.2 Multiple Access Schemes

The main three multiple access schemes are: TDMA, CDMA, and FDMA. Below is a brief description of the characteristics of each.

1.2.1 TDMA

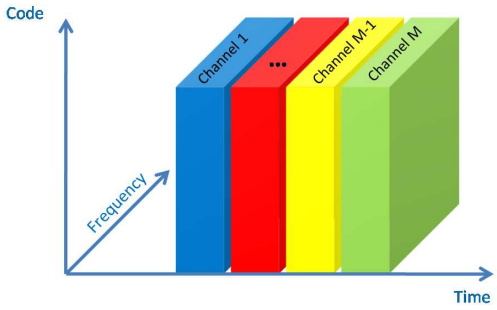

Figure 1.2. TDMA System.

In TDMA, time is divided into slots, where each user occupies the whole frequency spectrum at a specific time slot. To do its job properly, it requires time synchronization. A major advantage of TDMA is that users can operate at multiple data rates and this depends on how many time slots are assigned to each user. To decrease the interference between users, guard times are needed between the users' time slots.

1.2.2 CDMA

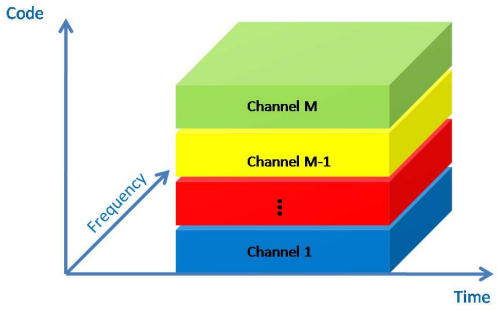

Figure 1.3. CDMA System.

In CDMA, users share the same channel in both time and frequency but they are differentiated from each other, by the unique code that is assigned to each user. So by assigning multiple codes to the same user, this will lead to increased data rates.

Power control in the uplink is a necessity to control the possible interference between the different users.

1.2.3 FDMA

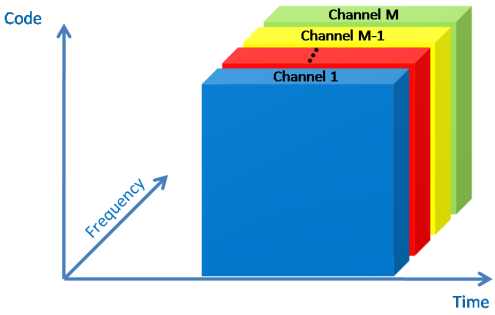

Figure 1.4. FDMA System.

In FDMA, the total available system bandwidth is divided into orthogonal frequency channels, where users transmit at the same time but each using the assigned frequency channel. Guard bands are needed to reduce the interference between the different users.

Orthogonal FDMA (OFDMA) is a modified version of FDMA which makes use of overlapping carrier frequencies to transmit data on thus increasing the data rates achieved per user, this issue that was difficult to achieve in the classical FDMA. Since the subcarriers are overlapping with minimum frequency separation, the spectral efficiency is very high compared to the conventional frequency division multiplexing (FDM) or FDMA where guard bands are required between the adjacent subcarriers.

Though it is highly spectral efficient, it still suffers from high peak-to-average power ratio (PAPR) which reduces the high power amplifiers (HPA) efficiency. The disadvantages are rectified by Single Carrier FDMA (SC-FDMA) which applies DFT-precoding to the conventional OFDMA systems.

Since these multiple access schemes involve multi-users, different subcarrier allocation schemes can be deployed. The possible allocation schemes are LFDMA where consecutive subcarriers are assigned to a user, B-IFDMA or B-EFDMA where interleaved blocks with a specific size are given to a user, and IFDMA where individual subcarriers with equidistant frequency spacing are allocated to a user. Each of these multiple access schemes offers a different trade-off between how much frequency diversity can be collected to take advantage of the fading channels, how much power amplifiers efficiencies can be reached, and how much performances can be achieved with the absence of proper channel knowledge at the receiver.

1.3 Scope

In this thesis, the wireless channel will be modeled emphasizing all the aspects of the challenges imposed like fading, inter-carrier interference (ICI), and inter-symbol interference (ISI). Multicarrier techniques (B-EFDMA) and Single Carrier techniques (IFDMA, LFDMA, and B-IFDMA) will be elucidated highlighting how these schemes exploit fading by collecting more frequency diversity, combat ISI and ICI. Schemes are compared at a Bit error rate (BER) basis, while taking into consideration the power amplifier efficiency achieved. After a careful study of the things affecting these performances, a set of parameters was devised. These parameters include the different multiple access schemes with different block sizes, the type of receiver equalizers, channel estimation methods, beside channel coding and modulation techniques.

End-to-end performance of each of these schemes are scrutinized under different deployment scenarios which were modeled by the different combinations of these parameters. And finally, the pros and cons of each scheme were shed light upon to understand which schemes and optimal parameters to be used in different scenarios.

1.4 Organization of this Thesis

The thesis is organized as follows:

Chapter 2 explores the behavior of the wireless channel and its statistical characterization. Two important phenomenon large scale and small scale fading based on channel variations with respect to distance are explained. Narrowband and wideband fading models are introduced and then the important characteristics of wideband channels like power delay profile, coherence bandwidth, Doppler power spectrum and coherence time are defined.

Chapter 3 gives an overview of the OFDM and OFDMA. Single Carrier with Frequency Domain Equalization (SC-FDE) and its multi-user version SC-FDMA are presented. The different mapping schemes are presented with their pros and cons on the trade-off between the frequency diversity collected, PAPR, and channel estimation performance. Moreover, the time domain behavior is elicited.

Chapter 4 introduces the importance of each of Convolutional and Turbo coding techniques in improving the BER performances. This will be followed by a brief explanation of the QPSK and 16-QAM modulations schemes. Finally, the pulse shaping technique to limit the bandwidth of the transmitted signal will be presented.

Chapter 5 presents the system model intended for the uplink multiple access scheme for IMT-Advanced and introduces the simulation parameters used in the thesis. Analysis has been done on PAPR and BER performances of the multiple access schemes in the presence and absence of perfect channel knowledge at the receiver.

Then conclusions will be drawn highlighting the optimal parameters.

Chapter 6 briefly highlights the main essence of the trade-off between the frequency diversity collected, the PAPR, and the channel estimation performance for the different mapping schemes.

Appendix A deals with the simulation of a time-frequency varying Rayleigh fading channel. The Spectrum method to generate the time-frequency fading samples based on Jake's or Clarke's doppler spectrum will been explained.

Appendix B presents more results to give more insight on understanding the performance behavior of the multiple access schemes under consideration.

2 MOBILE CHANNEL CHARACTERISTICS

Communications over mobile communication channel is a severe challenge since it is subjected to noise interference and more over the wireless channel undergo rapid changes in time due to mobility of user at vehicular speeds. Due to these rapid variations in behavior, a mobile channel is commonly called as Fading channel. So understanding the channel and its characteristics helps in designing a stable robust system with good performance. This chapter explores the behavior of wireless channel and statistical characterization of it. Important properties of wireless channel over time and frequency has been discussed in detail. Mainly a wireless channel is broadly classified in to two categories as large scale fading and small scale fading based on channel variations with respect to distance and are explained in the coming sections.

2.1 Large Scale Fading

Path loss and Shadowing vary over much longer distances hence they are called large scale propagation effects or large scale fading and are discussed in brief in this section.

2.1.1 Path Loss

Path loss is measured as a ratio of transmitted to received signal power and is dependent on the distance between transmitter and receiver. It is caused by effects of the propagation channel and gives received power variation with distance. For free space, path loss varies in direct proportion to the transmitter-receiver separation. Let P_t is the transmitted power of the signal and P_r is the received power of the signal then path loss P_L is defined as $P_L = P_t/P_r$ and path loss in dB is given as $P_L\,dB = 10\log_{10}(P_t/P_r)\,dB$. Empirical path loss models are available like Okumura, HATA and COperation européenne dans le domaine de la recherche Scientifique et Technique (COST) 231 which are based on extensive measurements (Goldsmith 2005).

2.1.2 Shadowing

A signal transmitted in a wireless medium is often obscured by obstacles between the transmitter and the receiver like mountains, buildings, furniture etc. The variations in the received signal power due to these obstructions is called shadow fading and it attenuates the received signal power. Various phenomenon that contribute to

shadowing are absorption, reflection, scattering and diffraction of the signal. Statistical model that describes this effect is log normal shadowing (Goldsmith 2005). In this model the ratio of transmit to receive signal power $\psi = P_t/P_r$ is distributed as log-normal in equation (2.1).

$$p_\psi \, dB = \frac{\xi}{\sqrt{2\pi}\sigma_{\psi_{dB}}} \psi \, exp \left[-\frac{(101og_{10}\psi - \mu_{\psi_{dB}})^2}{2\sigma^2_{\psi_{dB}}} \right], \psi > 0, \tag{2.1}$$

where $\xi = 10/ln10$, $\mu_{\psi_{dB}}$ is the mean of $\psi_{dB} = 101og_{10}\psi$ in dB and $\sigma_{\psi_{dB}}$ is the standard deviation of ψ_{dB} also in dB. Figure 2.1 shows the effect of path loss, shadowing and narrowband fading with distance . We can observe from the figure that shadowing varies slowly over the distance. Where as narrowband fading which is a particular case of small scale fading changes very rapidly with distance. The behavior of small scale fading and its properties are discussed in next section.

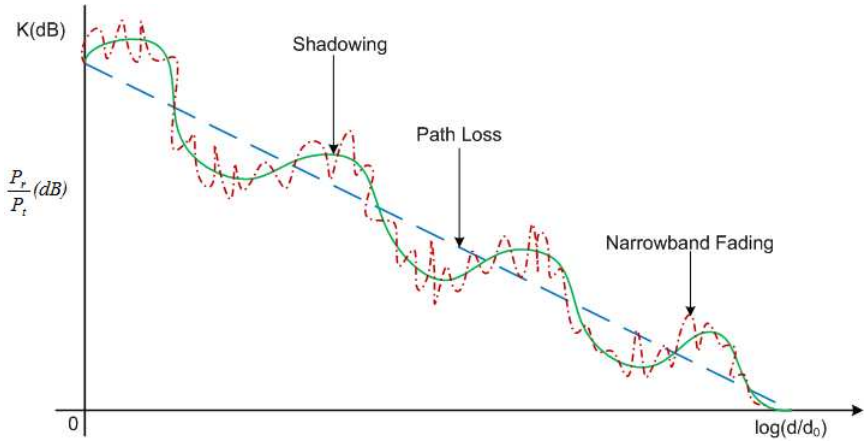

Figure 2.1. Combined Path Loss, Shadowing and Narrowband Fading.

2.2 Small Scale Fading

When a signal is transmitted over a wireless channel the signal will be reflected from the obstacles present in the channel. So instead of one copy of the transmitted signal, we receive multiple delayed copies of the same signal due to reflections from these physical barriers. These multiple copies of the same signal are commonly referred as multipath signal components. Figure 2.2 shows how multiple copies of the signal are generated at the receiver.

In figure 2.2.a we can observe that single pulse symbol transmitted over the multipath channel resulted in creation of four multipath components of the same pulse. The first component is the original pulse with out any reflections from obstacles and is known as line of sight component (LOS) (Sadeghi 2006). The time difference between arrival of the first multipath component of the signal and the last multipath

component of the signal is called maximum delay spread of the channel denoted by T_m. When we transmit more symbols in succession this multipath propagation leads to ISI between the transmitted symbols which can be inferred from figure 2.2.b and 2.2.c.

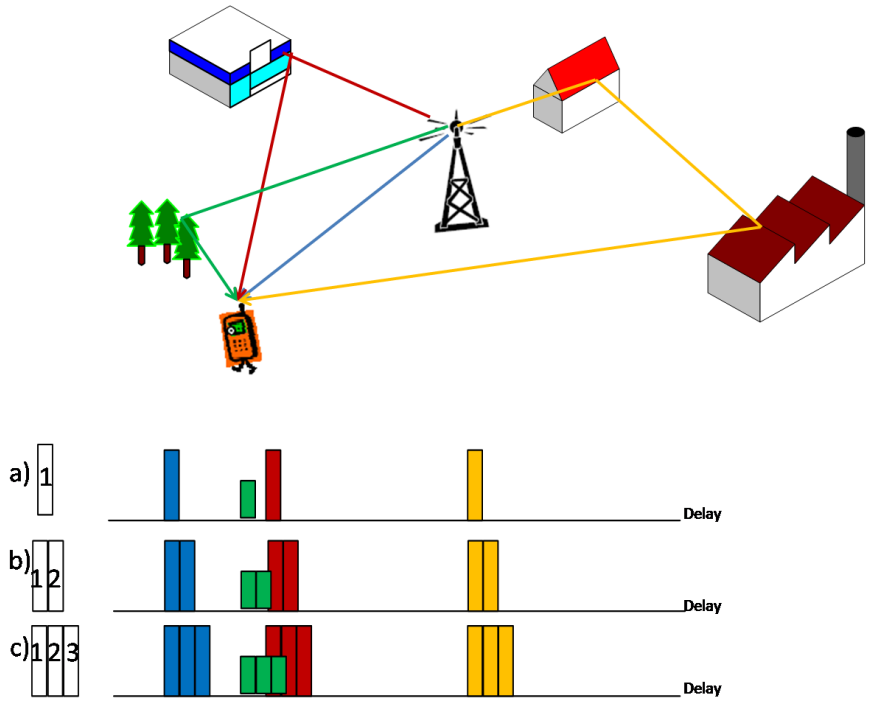

Figure 2.2. Multipath Channel.

Due to the constructive and destructive addition of these multipath signal components, the received signal strength varies very quickly over a small distance usually in the order of signal wavelength. Since the propagation channel varies over small distance it is called small scale fading.

Thus a single pulse transmitted over multipath propagation channel the received signal appears to be a pulse train at the receiver. As a result of it delay spread is introduced in the signal(Goldsmith 2005). More over mobility of the user incorporates time varying behavior to channel since the surroundings changes very quickly. When the receiver is in motion so does the hindrances in the channel changes in every moment of time. Small scale fading has been modeled as random time varying impulse response.

Small scale fading can be broadly classified in two categories as narrowband fading and wideband fading based on the relationship between signal bandwidth and maximum delay spread of the channel.

2.2.1 Narrowband Fading

Before going into details of time varying channel impulse response of narrowband fading let us introduce Doppler effect. Doppler shift is the change in frequency of the wave as observed by the receiver when it is moving towards or away from a source with some velocity. Doppler frequency f_D is defined as $f_D = \frac{v}{\lambda} cos(\theta)$, where v is the velocity of the receiver, λ is the wavelength and θ is the angle of arrival of the wave at the receiver.

The characteristics of multipath propagation channel can be studied by a simple geometrical model shown in figure 2.3. In this model the transmitter and receiver are considered to be at foci of an ellipsoid and receiver is moving with a velocity v along the foci of the ellipsoid (Ström 2008). Where each ellipsoid corresponds to a single scatterer or cluster of scatterers. Since the path lengths are equal in an ellipsoid so the delays corresponding to multipath components from a single scatterer are equal.

If there are more than one distinct scatterer in the channel, each one will be represented by an ellipsoid with a different delay as shown in figure 2.3(b). In narrowband fading $T_m \ll B^{-1}$ where B is the bandwidth of the transmitted signal, so the differential delay $\tau_1 - \tau_2$ are small compared to symbol duration hence all delays are approximately equal. On the other hand if the delays are resolvable $\tau_1 - \tau_2 \gg 1/B$ we have wideband fading which results in to a time dispersive or frequency selective channel and is discussed in detail in the coming sections (Ström 2008). As men-

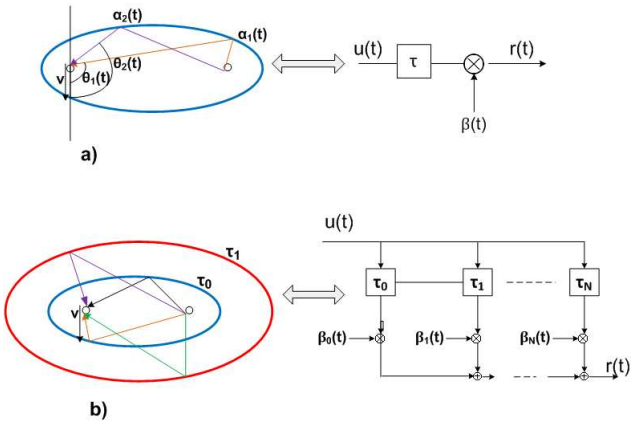

Figure 2.3. Ellipsoid Representation of Multipath Channel.

tioned earlier a transmitted signal will observe Doppler shift f_{Dn} due to the mobility of the terminal therefore for a transmitted signal $s(t) = Re\{u(t)e^{j2\pi f_c t}\}$ with M multipaths from a single scatterer in the channel each with path delay τ and reflection

coefficients $\alpha_n(t)$ the received signal is

$$\begin{aligned} r(t) &= Re\left\{\sum_{n=0}^{M} \alpha_n(t)\, u(t-\tau) e^{j2\pi[f_c+f_{Dn}(t)](t-\tau)}\right\}, f_{Dn} = \frac{v}{\lambda}\, cos(\theta_n) \\ &= Re\left\{e^{j2\pi f_c t}\, u(t-\tau) \sum_{n=0}^{M} \alpha_n(t)\, e^{j2\pi[f_{Dn}(t)(t-\tau)-f_c\tau]}\right\}, \\ &= Re\left\{e^{j2\pi f_c t}\, u(t-\tau)\beta(t)\right\}, \end{aligned} \tag{2.2}$$

where $u(t)$ is the complex baseband signal of the transmitted signal $s(t)$. $u(t)$ is commonly referred as complex envelope or complex lowpass equivalent signal of $s(t)$ and f_c is the carrier frequency, $\beta(t) = \sum_{n=0}^{M} \alpha_n(t) e^{j\phi_n(t)}$ and $\phi_n(t) = 2\pi[f_{Dn}(t)(t-\tau) - f_c\tau]$.

For a channel with single scatterer with large number of multipaths and none of the multipath is dominating we can invoke the central limit theorem and can model $\beta(t)$ as a complex Gaussian random variable. Where the real and imaginary parts of $\beta(t)$ are independent Gaussian random variables with zero mean and variance σ^2. The envelope $z(t) = |\beta(t)| = \sqrt{Re(\beta(t))^2 + Im(\beta(t))^2}$ has a Rayleigh distribution. On the other hand if any one of the multipath components is dominating then $\beta(t)$ is modeled as complex Gaussian random variable with non zero mean thus the envelope $z(t)$ is Ricean distributed.

Narrowband fading can be modeled practically by Clarke's or Jake's model. In Clarke's or Jake's model of narrowband fading it has been assumed that all the multipath components arrive with same average power and components arrive uniformly with same angle of arrival (Ström 2008). Using this model, it can be shown that autocorrelation and power spectral density of narrowband fading process are related as in equation (2.3) and they constitute a fourier transform pair.

$$A_\beta(\tau) = C\, J_0(2\pi f_{Dmax}\tau) \longleftrightarrow S_\beta(f) = \begin{cases} \frac{1}{\pi f_{Dmax}} \frac{C}{\sqrt{1-(f/f_{Dmax})^2}}, |f| \le f_{Dmax} \\ 0\, otherwise. \end{cases} \tag{2.3}$$

where f_{Dmax} is the maximum Doppler frequency, C is constant related to average received power and $J_0(x)$ is Bessel function of first kind of zero order. Figure 2.4 shows the power spectral density and autocorrelation of Clarke's or Jake's model and the spectrum is commonly known as Clarke's or Jake's spectrum.

2.2.2 Wideband Fading

In the other category of small scale fading known as wideband fading in which we observe another kind of distortion due to multipath delay spread when the signal bandwidth is approximately equal to inverse of delay spread $B \approx 1/T_m$. The difference between narrowband and wideband fading models can be observed from the figure 2.5.

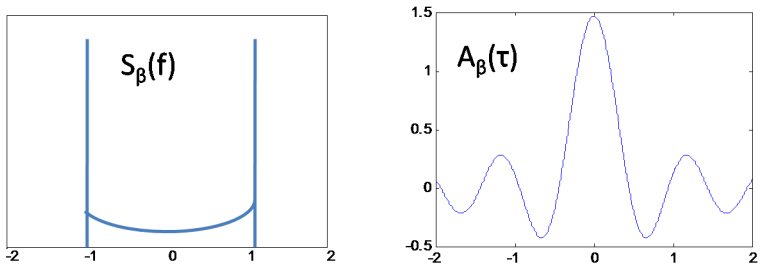

Figure 2.4. PSD and Autocorrelation of $\beta(t)$ for Clarke's Model.

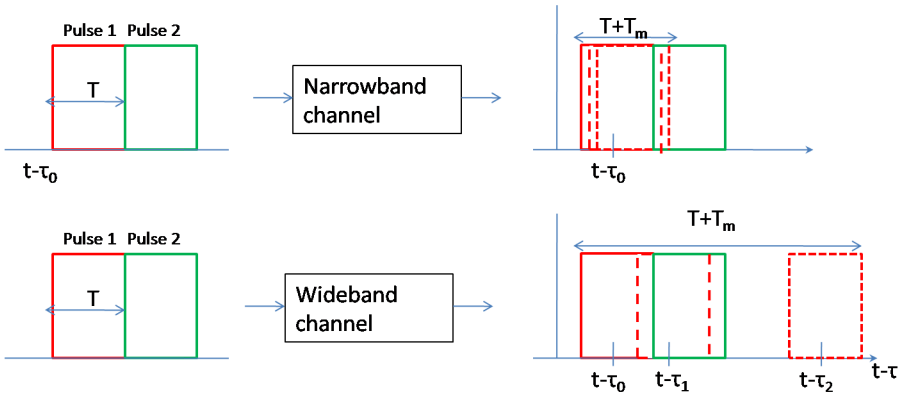

Figure 2.5. Comparison of Narrowband and Wideband Fading Models.

A short transmitted pulse of duration T results a signal of duration $T + T_m$ in a multipath channel. As we can observe in the case of narrowband fading where the symbol duration $T \gg T_m$ the multipath components are received roughly on top of one another so little time spreading of the pulse therefore little interference with the subsequent transmitted pulses (Goldsmith 2005). Alternatively in wideband fading the symbol duration $T \approx T_m$ so the duration of the received pulse is considerably increased as a result it interferes with the subsequent transmitted pulses thus causing ISI. The idea behind multicarrier modulation techniques like OFDM is to change the characteristics of transmitted signal by elongating the symbol duration mainly to overcome ISI.

Narrowband fading processes can be described completely by their autocorrelation or power spectral density. For wideband signals amplitude and phase distributions are not enough to characterize since they also get effected by multipath distortion. So the effect of multipath delay spread and time variations must be taken in to account while describing the wideband fading processes.

Wideband channels are usually characterized by time-varying impulse response and time-varying frequency response. Time-varying impulse response $c(\tau, t)$ is modeled as two-dimensional random process and time-varying frequency response $C(f, t)$ is

obtained from $c(\tau, t)$ by taking fourier transform with respect to τ i.e, $C(f, t) = F_\tau[c(\tau, t)]$ (Ström 2008). An example of two dimensional discrete-time varying impulse response $c(\tau, t)$ is shown in figure 2.6 (Rappaport 2002).

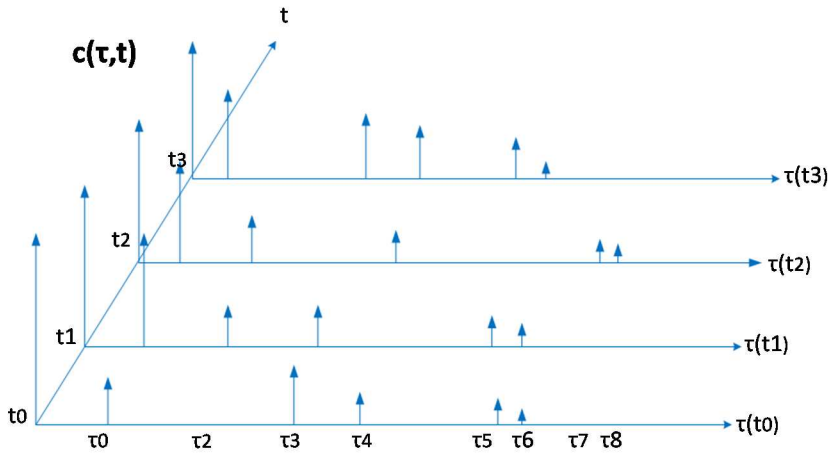

Figure 2.6. Time-Varying Discrete-Time Impulse Response Model for a Multipath Channel

We often assume the channel to be wide sense stationary (WSS) with uncorrelated scattering. Wide sense stationary channel means that channel statistics measured at two different points in time is dependent only on their time difference and is completely independent on time index when it is observed. So for a WSS channel the time-varying channel impulse response $c(\tau, t)$ is a random process in t. Uncorrelated scattering means the channel response $c(\tau_1, t)$ observed for multipath component τ_1 is uncorrelated with channel response $c(\tau_2, t)$ corresponding to multipath delay τ_2 and $\tau_1 \neq \tau_2$.

For WSS-US channel the autocorrelation function of time-varying impulse response $A_c(\tau; \Delta t)$ and autocorrelation function of time-varying frequency response $A_C(\Delta f; \Delta t)$ are given in equation (2.4) and equation (2.5) respectively.

$$A_c(\tau; \Delta t) = E[c^*(\tau_1; t)\, c(\tau_2; t + \Delta t)]. \quad (2.4)$$

$$A_C(\Delta f; \Delta t) = E[C^*(f; t)\, C(f + \Delta f; t + \Delta t)]. \quad (2.5)$$

$A_c(\tau; \Delta t)$ gives average output power associated with the channel as function of multipath delay and observation time difference where as $A_C(\Delta f; \Delta t)$ determines average output power associated with the channel as function of observation time and frequency difference. There is one more function that characterizes the average power associated with the channel as a function of multipath delay τ and Doppler frequency ρ (Goldsmith 2005). It is called scattering function $S_c(\tau, \rho)$ and is obtained from $A_c(\tau; \Delta t)$ by taking Fourier transform with respect to time difference parameter Δt.

The characteristics of wideband channel are defined mainly on autocorrelation and scattering function of channel response and are discussed in detail in next section. While the simulation of wideband channel model is explained clearly in Appendix A.

2.3 Characteristics of Wideband Fading

The most important characteristics of a wideband channel are power delay profile, coherence bandwidth, Doppler power spectrum and coherence time. These characteristics are defined based on channel autocorrelation or scattering function.

2.3.1 Power Delay Profile

Power delay profile represents the average power associated with each multipath delay component. It represents the strength of multipath components and their corresponding delays in the channel so it's also referred as multipath intensity profile. It is defined as the autocorrelation equation (2.4) with $\Delta t = 0$ then $A_c(\tau) = A_c(\tau; 0)$ thus it represents the channel variations corresponding to delay spread.

There are various ways to describe the channel delay spread, the two most popular ones used much often in practice are average delay spread (μ_{Tm}) and Root mean square (RMS) delay spread (σ_{Tm}). They can be analyzed from power delay profile and are defined empirically in equation (2.6).

$$\mu_{Tm} = \frac{\int_0^\infty \tau A_c(\tau)}{\int_0^\infty A_c(\tau)}, \quad \sigma_{Tm} = \sqrt{\frac{\int_0^\infty (\tau - \mu_{Tm})^2 A_c(\tau)}{\int_0^\infty A_c(\tau)}}. \tag{2.6}$$

With channels having large number of scatterers it is observed that mean delay spread is approximately equal to RMS delay spread i.e, $\mu_{Tm} \approx \sigma_{Tm}$. Another way to describe the delay spread is maximum delay spread T_m . It is defined as the maximum delay after which the strength of the multipath components is negligible, mathematically for $\tau \geq T_m, A_c(\tau) \approx 0$. We use the terms μ_{Tm}, σ_{Tm} and T_m interchangeably in this report without loss of generality in analyzing things.

Whether a multipath propagation channel introduces ISI or not to transmitted signal can be studied from the power delay profile. Received signals would not experience much ISI if their symbol duration T is much larger than RMS delay spread i.e, for $T \gg \sigma_{Tm}$. On the other hand they experience significant ISI if symbol duration is less than the RMS delay spread, $T \ll \sigma_{Tm}$.

The power delay profile of the WINNER C2 NLOS channel (Baum *et al.* Nov. 2005) that is used in this thesis is given in table 2.1. The normalized power delay profile of WINNER C2 NLOS channel is shown in figure 2.7.

Delay [ns]	Power [dB]	Delay [ns]	Power [dB]
0	-0.5	650	-7.4
5	0.0	670	-8.4
135	-3.4	720	-11.0
160	-2.8	750	-9.0
215	-4.6	800	-5.1
260	-0.9	945	-6.7
385	-6.7	1035	-12.1
400	-4.5	1185	-13.2
530	-9.0	1390	-13.7
540	-7.8	1470	-19.8

Table 2.1. WINNER C2 NLOS Power Delay Profile.

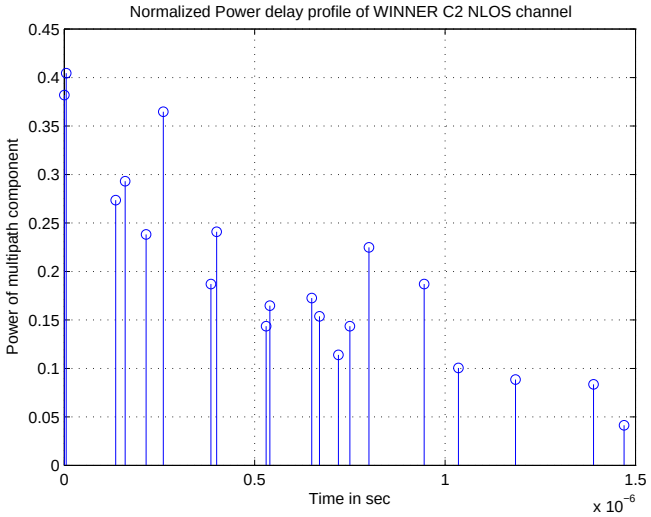

Figure 2.7. Normalized Power Delay Profile of Winner C2 NLOS Channel.

2.3.2 Coherence Bandwidth

The spaced-frequency correlation function $A_C(\Delta f)$ is the Fourier transform of the power delay profile with respect to τ therefore $A_C(\Delta f) = F_\tau[A_c(\tau)]$. It is defined as the autocorrelation equation (2.5) with $\Delta t = 0$ then $A_C(\Delta f) = A_C(\Delta f; 0)$.

Coherence bandwidth is the range of frequencies over which the channel passes all spectral components with almost equal gain and linear phase (Rappaport 2002). It is also the band of frequencies over which the channel is highly correlated in frequency. Coherence bandwidth is the frequency B_c at which the $A_C(\Delta f) \approx 0$ for $\Delta f \geq B_c$ and is inversely related to the maximum delay spread of the channel as $B_c \approx 1/T_m$. This means channel goes in to a new realization in frequency after every B_c in other words with-in B_c the fading gain is almost equal.

So for a signal if its bandwidth is much less than the coherence bandwidth i.e; $B \ll B_c$ then fading is roughly equal over the entire signal bandwidth, this type of fading is called flat fading. Alternatively if $B \gg B_c$ then fading gain varies widely over the signal bandwidth in this case its called frequency selective since fading is selective over frequencies of the signal bandwidth.

In flat fading the signal experiences negligible ISI since $T_s \approx 1/B \gg 1/B_c \approx \sigma_{Tm}$. On the other hand signal experiences considerable ISI in frequency selective fading because $T_s \approx 1/B \ll 1/B_c \approx \sigma_{Tm}$. The relationship between the power delay profile and coherence bandwidth is shown in figure 2.8.

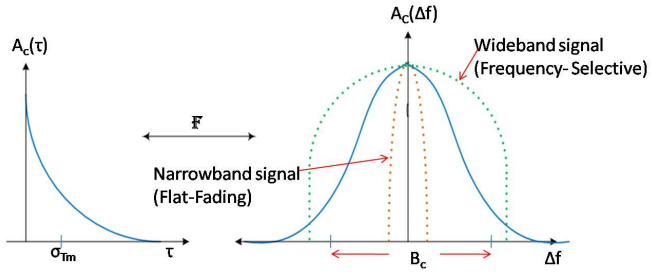

Figure 2.8. Power Delay Profile and Coherence Bandwidth.

2.3.3 Doppler Power Spectrum and Coherence Time

Doppler power spectrum characterizes the channel variations which occur due to movement of transmitter or receiver. Due to this mobility we observe a shift in the frequency of received signal commonly referred to as Doppler shift.

This doppler effect can be measured by taking the Fourier transform of $A_C(\Delta f; \Delta t)$ with respect to Δt so $S_C(\Delta f; \rho) = F_{\Delta t}[A_C(\Delta f; \Delta t)]$. $S_C(\rho) \triangleq S_C(0; \rho)$ characterizes doppler shift for a single frequency and $A_C(\Delta t) \triangleq A_C(\Delta f = 0; \Delta t)$ describes the behavior of the autocorrelation function with time and is used in defining the Coherence time.

Coherence time T_c describes how the channel decorrelates over time. It is defined as the range of values over which $A_C(\Delta t)$ is approximately nonzero. So after every T_c seconds the channel observes a new realization in time. Hence if the symbol duration $T_s \ll T_c$ then the channel impulse response is time invariant over one symbol period, so its called slow fading. Conversely if the symbol duration $T_s \gg T_c$ then channel impulse response varies rapidly in one symbol period for this reason it is known as fast fading.

Doppler spread B_D is defined as the maximum ρ at which the magnitude of the doppler spectrum is nearly zero and is inversely related to channel coherence time as $B_D \approx 1/T_c$. Figure 2.9 shows how coherence time and doppler power spectrum are related.

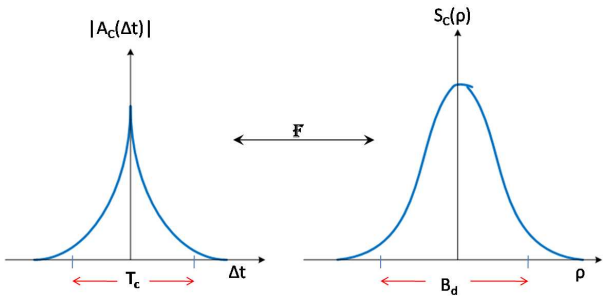

Figure 2.9. Doppler Power Spectrum and Coherence Time.

A summary of different classifications of the time frequency varying channel based on its characteristics relative to signal characteristics is given in figure 2.10 (Rappaport 2002). A summary of fading channel manifestations is given in figure 2.11 (Sklar 1997).

Small Scale Fading

(Based on multipath time delay spread)

Flat Fading	Frequency Selective Fading
1. BW of signal < Bc of channel	1. BW of signal > Bc of channel
2. Delay Spread < Symbol period	2. Delay Spread > Symbol period

Small Scale Fading

(Based on Doppler spread)

Fast Fading	Slow Fading
1. High Doppler spread	1. Low Doppler spread
2. Coherence Time < Symbol period	2. Coherence Time > Symbol period
3. Channel variations faster than baseband signal variations.	3. Channel variations slower than baseband signal variations.

Figure 2.10. Summary of Classification of the Channels.

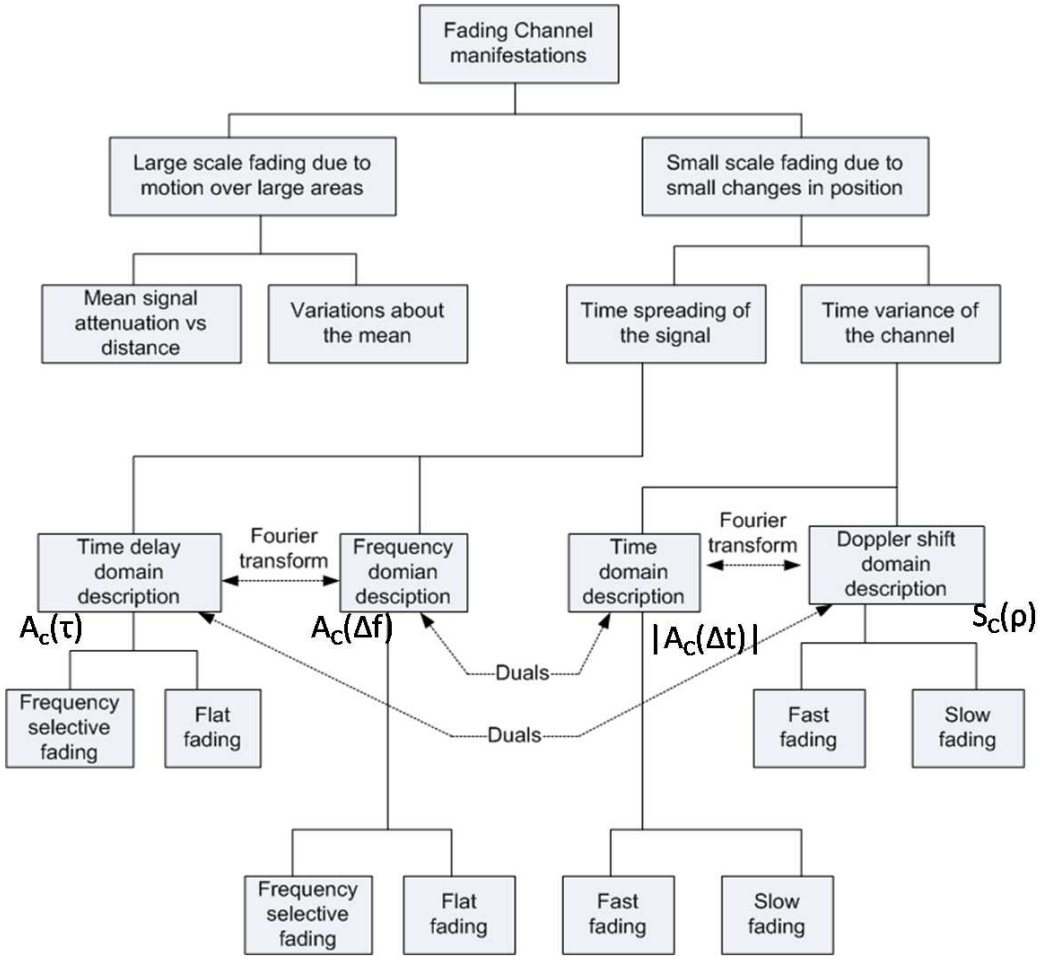

Figure 2.11. Fading Channel Manifestations.

3 OFDMA AND SINGLE CARRIER FDMA

To better exploit the characteristics of the wireless communication channels and mitigate the level of challenges imposed by the frequency-selective fading, different frequency multiplexing/multiple-access techniques can be used.

In this chapter, we will give an overview of the popular Orthogonal Frequency Division Multiplexing (OFDM) multicarrier modulation scheme, and its multi-user version which is called Orthogonal Frequency Division Multiple Access (OFDMA). Also, we will describe Single Carrier with Frequency Domain Equalization (SC-FDE) which is a modified version of OFDM, and we will present its multi-user version Single Carrier Frequency Division Multiple Access (SC-FDMA), an attractive option and a working assumption for the uplink in 3GPP Long Term Evolution (LTE) (The 3rd Generation Partnership Project (3GPP) 2006). Moreover, the pros and cons of each of the techniques will be elicited.

3.1 OFDM and OFDMA

In response to the frequency-selective fading in wideband channels that was described in the previous chapter, OFDM comes into the picture. It is a multicarrier modulation technique which subdivides the Bandwidth into smaller orthogonal subcarriers which are used to carry the transmitted information. The main concept behind this segregation is to have subcarrier bandwidth smaller than the coherence bandwidth. In this case each subchannel is seen as a flat fading channel by the corresponding subcarrier and this simplifies the equalization process which will be discussed in the coming chapters (Myung and Goodman 2008).

Figure 3.1 shows the spectrum of ten orthogonal subcarriers in one OFDM symbol assuming that each OFDM symbol carries ten baseband modulated symbols on its ten subcarriers. Since the subcarriers are overlapping with minimum frequency separation, the spectral efficiency is very high compared to the conventional frequency division multiplexing (FDM) where guard bands are required between the adjacent subcarriers.

In the time domain, OFDM is also advantageous. It divides a high-rate digital data stream into a number of lower-rate data streams which are transmitted in parallel on the different subcarriers. Having enough slow narrow band signals, the symbol duration in each one will be long enough. As seen in the earlier chapter, having symbol duration larger than the maximum delay spread helps to eliminate intersymbol interference (ISI) (Myung and Goodman 2008), and thus OFDM exploits this property in the time domain.

The essential elements of an OFDM transmitter and receiver are shown in figure 3.2

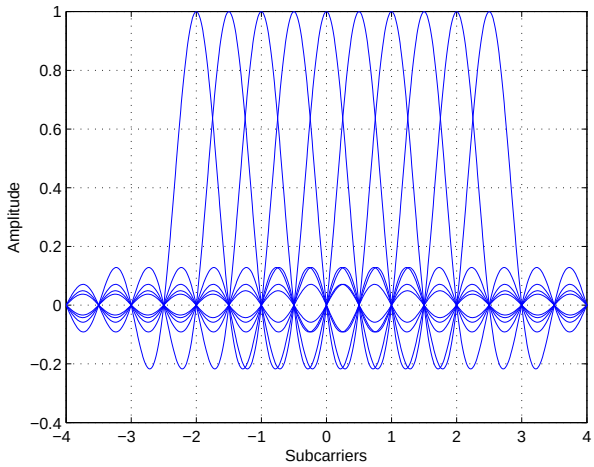

Figure 3.1. Orthogonal Subcarriers in OFDM.

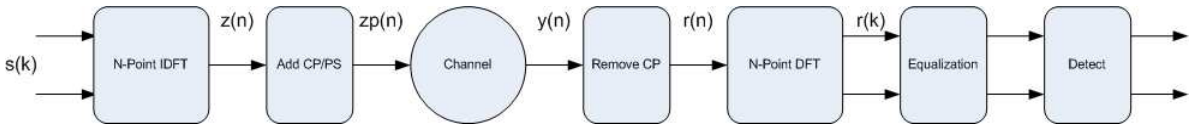

Figure 3.2. OFDM Transceiver.

where the channel block includes the channel impulse response $h(n)$, and the Additive White Gaussian noise $w(n)$.

The heart of the OFDM transmitter in the Inverse Discrete Fourier Transform (IDFT) which is an easy mechanism to convert the N coded baseband modulated symbols $s(k)$ carried on the available subcarriers to one time domain symbol $z(n)$ which is transmitted sequentially.

$$z(n) = \frac{1}{N} \sum_{k=0}^{N-1} s(k) e^{j2\pi k \frac{n}{N}}. \tag{3.1}$$

This step is followed by adding a cyclic prefix, where the last u samples of the sequence $z(n)$ are appended to the beginning of the sequence. This cyclic prefix could be considered as a guard duration between the OFDM symbols. If the cyclic prefix duration is greater or equal to the channel delay spread T_m, then the first u samples of the channel output of each of the transmitted symbols that are affected by ISI can be discarded without losing the original information sequence. Also pulse shaping is applied in order to reduce out-of-band interference and as a result side lobes in the frequency domain will be decreased.

One of the main reasons to append the last part of the block to the beginning is because of the fact that when the data stream $zp(n)$ is sent through the linear time-invariant discrete-time channel $h(n)$, the output $y(n)$ will be an N-point circular convolution.

$$\begin{aligned} y(n) &= zp(n) \bigotimes h(n) + w(n) \\ &= h(n) \bigotimes zp(n) + w(n) \\ &= \sum_k h(k) zp(n-k)_N + w(n), \qquad n = 0, ..., N-1, \end{aligned} \tag{3.2}$$

where $(n-k)_N$ denotes $(n-k)$ modulo N which means that $zp(n-k)_N$ is a periodic version of $zp(n-k)$ with period N, and $w(n)$ is white Gaussian noise.

At the receiver, the cyclic prefix is removed thus discarding the samples which are affected by ISI. Then DFT is applied on $r(n)$ to move back to the frequency domain. From the definition of DFT, circular convolution in time domain leads to multiplication in the frequency domain (Goldsmith 2005) as shown in equation 3.3.

$$r(k) = DFT\{r(n)\} = \sum_{n=0}^{N-1} r(n) e^{-j2\pi k \frac{n}{N}} = H(k)s(k) + n(k). \tag{3.3}$$

where n(k) is the noise in the frequency domain.

Whether we have perfect channel knowledge at the receiver or estimated channel in frequency domain, $r(k)$ is equalized using any of the available equalization methods. A simple way to recover the transmitted $s(k)$ is to multiply $r(k)$ by the complex conjugate of the channel gain.

$$H(k)^* r(k) = H(k)^* H(k) s(k) + H(k)^* n(k) = |H(k)|^2 \tilde{s} + H(k)^* n(k), \tag{3.4}$$

where $\tilde{s}$ is a modified version of the input symbols s.

Hence the angle of the complex number $H(k)^* r(k)$ is equal to the angle of $s(k)$ which implies that the bits are correctly detected and decoded if the noise level is small.

An OFDM symbol holds data for one user, but to accommodate multiple users simultaneously, OFDMA is used. In the downlink, one OFDM symbol holds data for multiple users where each mobile terminal will pick up the data carried on the subcarriers that are assigned to it. Figure 3.3 shows an example of one OFDM symbol holding data for 3 users following a localized allocation scheme.

In the uplink, things are a bit different, since each user will send an OFDMA symbol where only the assigned subcarriers are used to carry the data and the rest carry nothing (Myung *et al.* 2006) as shown in figure 3.4.

Figure 3.5 shows the block diagram of OFDMA which is similar to that of OFDM but there is an extra step at the transmitter where the user maps the K transmitted

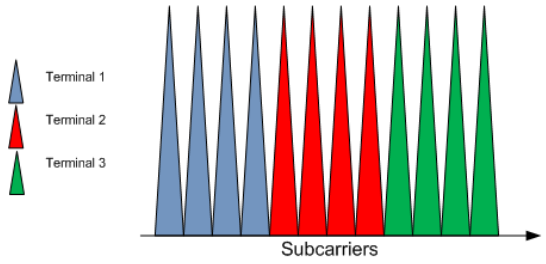

Figure 3.3. Downlink OFDM Subcarrier Allocation for 3 Users.

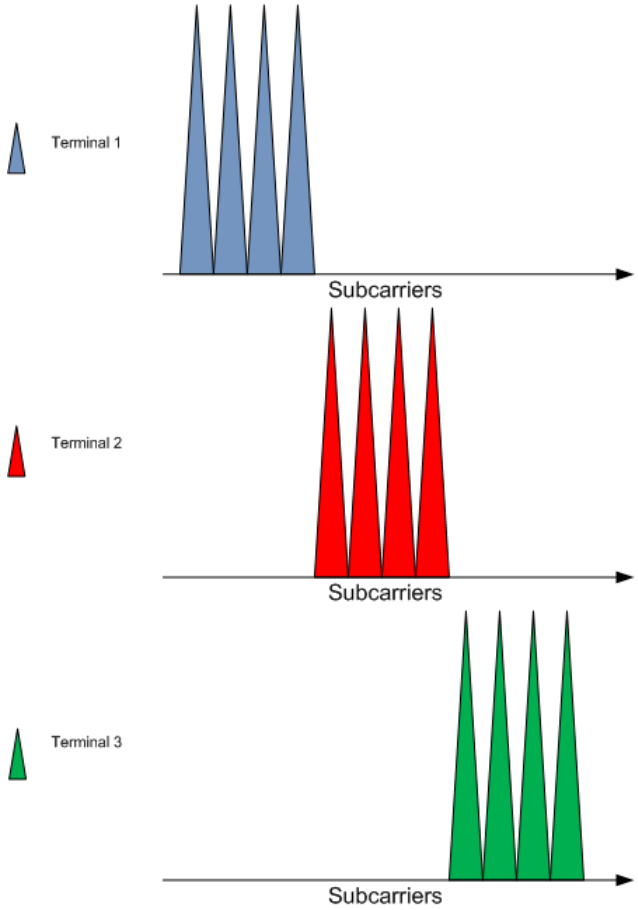

Figure 3.4. Uplink OFDMA Subcarrier Allocation for 3 Users.

symbols to M locations, where $k = 0..K-1$, $K < M$ and M is the length of the transmitted OFDM symbol. Therefore, only K out of M subcarriers carry information and are nonzero. Also, the receiver has to do subcarrier demapping to extract the information for a certain user. There are different mapping schemes where some are advantageous over the others since they collect more frequency diversity or have lower PAPR or perform better under imperfect CSIR but these different mappings will be discussed in the next section.

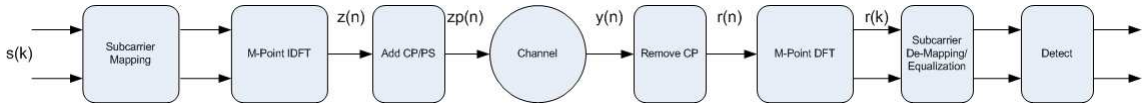

Figure 3.5. OFDMA Transceiver.

3.1.1 Pros & Cons

As we saw earlier, a major advantage of OFDM/OFDMA in broadband systems is the mitigation of ISI. This advantage by itself decreases drastically the signal processing complexity at the receiver's side since there is no need for high complexity equalizers. Moreover, the spectral efficiency is high because of the overlapping orthogonal subcarriers in the frequency domain as shown in figure 3.1.

Also, system throughput can be significantly improved by adapting the data rate per subcarrier based on the channel knowledge and the signal-to-noise ratio (SNR) corresponding to that subcarrier (Myung and Goodman 2008).

Since the modulation and demodulation are implemented using IDFT and DFT respectively, Fast Fourier Transform (FFT), which is an efficient algorithm to compute IDFT and DFT, can be used to increase the efficiency of the system.

Finally, for a given channel delay spread, the receiver complexity is much lower than a single carrier system with a time domain equalizer (Myung and Goodman 2008).

Despite these advantages, OFDM/OFDMA suffer from several drawbacks. A major weakness is the high peak-to-average power ratio (PAPR) which decreases the efficiency of the power amplifiers used. The reason for such a high PAPR is because the transmitted signal is a superposition of all the subcarriers with different carrier frequencies thus high amplitude peaks are inevitable. Figure 3.6 shows the modulation over 4 subcarriers where all the subcarriers have the same amplitude. But after superposition, we see that the combined curve in figure 3.7 shows how much the signal varies compared to the underlying constant subcarrier's amplitude (Rumney 2008).

Also, frequency offsets in the subcarriers might destroy the orthogonality property thus causing intercarrier interference (ICI).

Finally, adaptive or coded schemes are a necessity or else spectral nulls in the channel will destroy the data of the subcarrier and there will be no way to recover the data.

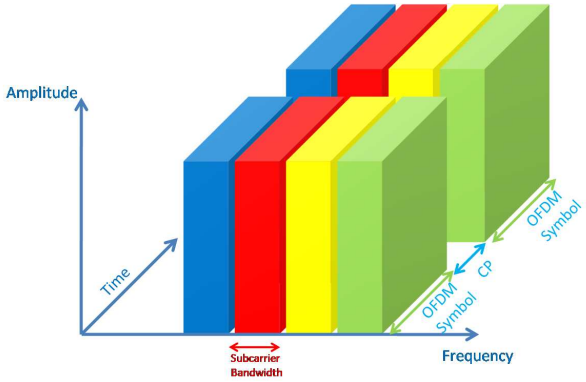

Figure 3.6. OFDM Modulation on the Different Subcarriers.

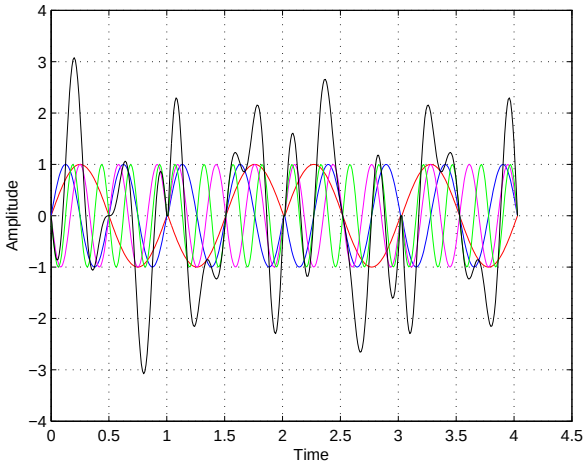

Figure 3.7. Superposition of Subcarriers with Different Carrier Frequencies.

3.2 SC-FDE and SC-FDMA

Another alternative to multicarrier modulation techniques is the use of single carriers techniques but with frequency domain equalization and that is because of the impracticality and complexity of time domain equalizers. It is another way to take advantage of the frequency selectivity thus delivering the same overall performance with the same overall complexity compared to OFDM schemes. Figure 3.8 shows the difference between OFDM and SC-FDE transceivers where the IDFT in SC-FDE transmitter is moved to the receiver. So the symbols that we would like to transmit are considered as the time domain symbols. At the receiver, the time domain signal is transformed to the frequency domain where equalization is done and back to the time domain using the IDFT block where detection occurs.

Having a system with the same overall complexity, offering the same performance

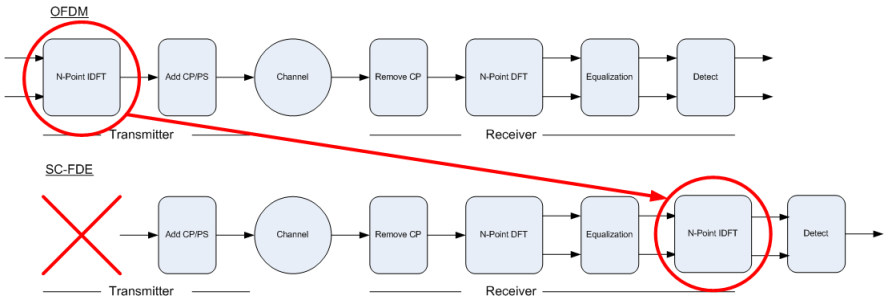

Figure 3.8. OFDM and SC-FDE Transceiver.

but providing low PAPR because of the single carrier modulation at the transmitter seems to be a better alternative for the uplink in IMT-Advanced. Figure 3.9 shows how the symbols will be transmitted, and basically there is no addition of different signals to get to the time domain signals, and that is why we have low PAPR (Rumney 2008).

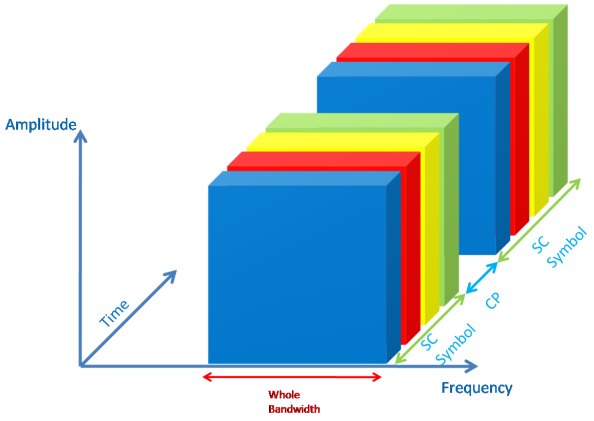

Figure 3.9. Single Carrier Modulation with Frequency Division Multiplexing.

And since we are using the whole bandwith for each symbol, the system has a high immunity against frequency selective fading since it collects frequency diversity. But looking at figure 3.9, we can see that the time domain symbols are shorter thus Inter-Symbol Interference (ISI) is introduced, and the use of equalizers become a necessity to mitigate the effect of ISI.

Same thing goes for Single Carrier Frequency Division Multiple Access (SC-FDMA) which is the multi-user version of SC-FDE making it the direct alternative to OFDMA for the uplink. It is a modified version of OFDMA and it is known as DFT-precoded OFDMA. Figure 3.10 shows the block diagram of SC-FDMA where we see two extra modules (DFT in the transmitter and IDFT in the receiver) which makes it different from the OFDMA block diagram.

So we start with the time domain symbols $s(k)$, take K-point DFT to move to the

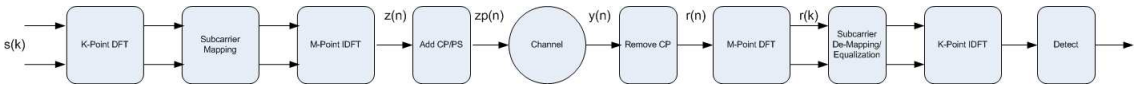

Figure 3.10. SC-FDMA Block Diagram.

frequency domain where we accommodate to the other users in the system by adding zeros on the subcarriers which are reserved for them, then M-point IDFT transforms it to the time domain, where cyclic prefix is added and transmission occurs. At the receiver, cyclic prefix is removed, followed by M-point DFT to move back to the frequency domain where the data on the subcarriers specific to a user are extracted, equalized, and then K-point IDFT moved the signal back to the time domain where detection occurs.

But the most important module is the subcarrier mapping since it governs the trade-off between how much frequency diversity can be collected, how much power amplifier efficiency can be achieved, and how much Bit Error Rate (BER) performance can be reached in the absence of channel knowledge at the receiver.

3.2.1 Subcarrier Mapping

The two main subcarrier mappings are the Interleaved and Localized FDMA as shown in figure 3.11 (Svensson *et al.* 2007). In the former, subcarriers with equidistant frequency spacings are allocated to users whereas in the latter, consecutive subcarriers or one chunk are allocated to users. A chunk is defined as a time-frequency unit where the subcarriers included experiences flat fading even in largely frequency selective channels and users at vehicular speeds.

It is obvious that IFDMA is a scheme which collects lots of diversity thus giving very good BER performances but the pilot overhead to estimate the channel is increased. On the other hand, LFDMA does not collect as much diversity as IFDMA schemes but they reduce the pilot overhead to estimate the channel since interpolation in the frequency domain is possible.

To illustrate how the mapping works, figure 3.12 show an example with a time domain signal x_n of length 4 and its frequency domain representation X_k after applying the DFT-precoding step. The two types of mapping which were defined above where the total length of the SC-FDMA symbol is 12 meaning that 2 other users can be accommodated (Myung and Goodman 2008).

Block interleaved FDMA (B-IFDMA), the mapping scheme that was introduced in (Svensson *et al.* 2007), is a generalization of both schemes trying to combine the advantages that IFDMA and LFDMA offers. In this mapping scheme, multiple blocks with equidistant frequency spacing are allocated to users, where each block consists of few number of consecutive subcarriers over few SC-FDMA symbols in

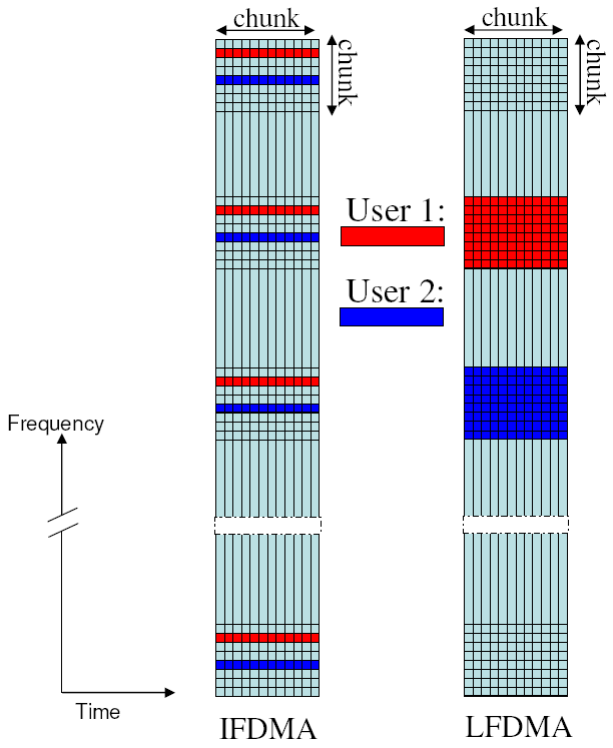

Figure 3.11. Subcarrier Mapping for IFDMA and LFDMA.

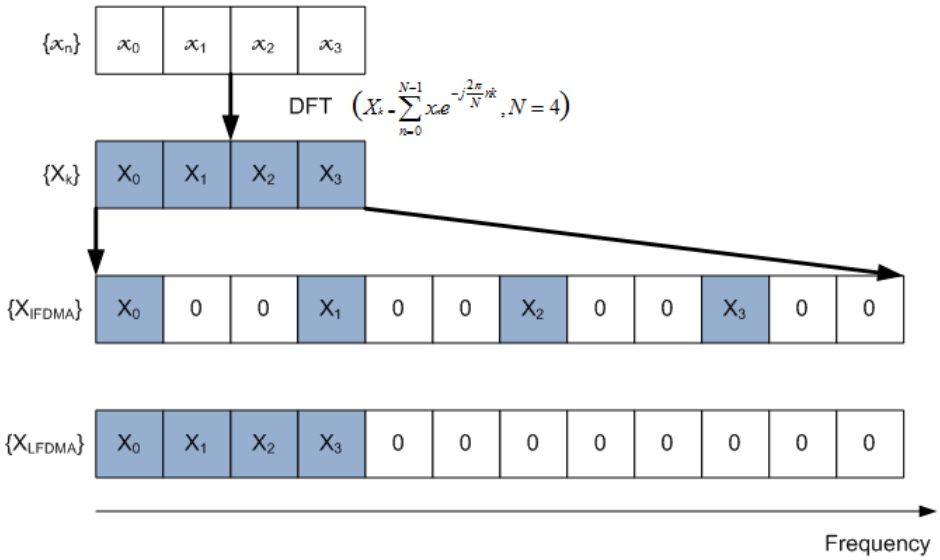

Figure 3.12. Example of IFDMA and LFDMA Mapping.

time. Figure 3.13 shows how subcarriers are allocated. A continuation of the previous example to show what happens when we deploy B-IFDMA schemes for block size 2 is shown in figure 3.14.

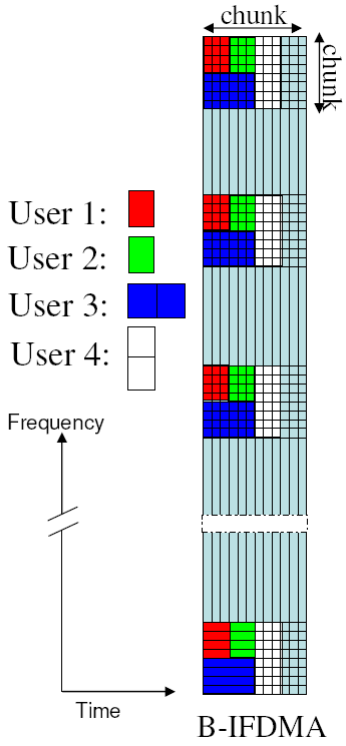

Figure 3.13. Subcarrier Mapping for B-IFDMA.

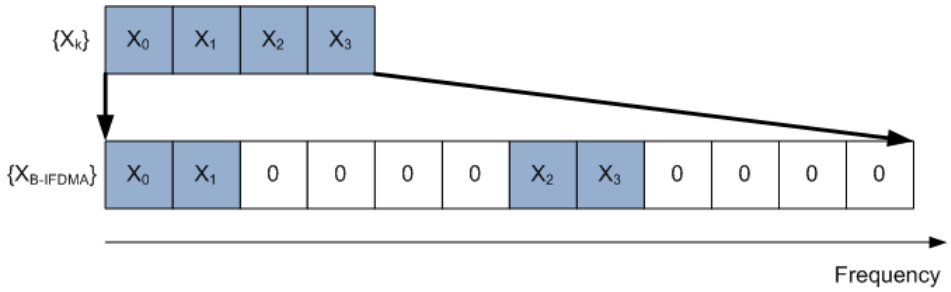

Figure 3.14. Example of B-IFDMA mapping.

3.2.2 Time Domain Representation

In this section, we will give an insight at the time domain signal after the IDFT at the transmitter side for the three mapping schemes that were introduced before. Looking at the time domain signal, we can get an essence of why different mapping schemes have different PAPR in the absence of pulse shaping which will be touched on in the following chapter.

For the case of IFDMA, the resulting time domain signals of the example in figure 3.12 are nothing but Q repetitions of the original signal scaled by a factor of $\frac{1}{Q}$

where Q is the number of users in the system and this is shown in figure 3.15.

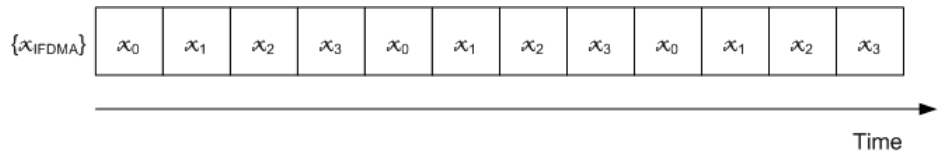

Figure 3.15. Time Domain Symbols of IFDMA.

When the subcarrier allocation starts from the r^th subcarrier instead of starting from the 0^{th} subcarrier as in figure 3.12, there is an additional phase rotation to the Q repetitions of the original signals which are scaled by the factor $\frac{1}{Q}$. In (Myung and Goodman 2008), there is a mathematical derivation of each of the cases.

In the case of LFDMA, the time domain signals as shown in figure 3.16 has the exact copies of the input symbols with a scaling factor of $\frac{1}{Q}$ at sample positions that are integer multiples of Q where Q is the number of users. The values in between these positions are a combination of all the symbols with different complex weighting. Mathematical derivations are found in (Myung and Goodman 2008). Lastly, the

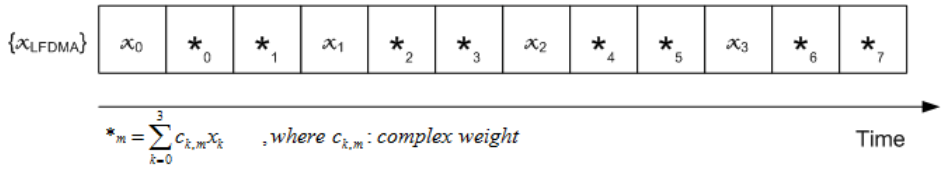

Figure 3.16. Time Domain Symbols of LFDMA.

time domain symbols of B-IFDMA in this example, is the same as the time domain signals in the LFDMA case where it contains exact copies of the input symbols with a scaling factor of $\frac{1}{Q}$ at sample positions that are integer multiples of Q where Q is the number of users. But the in-between values are complex weighted and different from the LFDMA case.

3.3 Summary

In this chapter, we saw the advantages of OFDM/OFDMA systems and the way they improve spectral efficiency, mitigate ISI, and take advantage of the frequency selective channel. Despite these advantages, OFDM/OFDMA suffers from high PAPR which is a critical constraint in the uplink. They also suffer from frequency offsets and the use of coded schemes is a necessity.

On the other hand, SC-FDE/SC-FDMA is another way to take advantage of the frequency selective channels while having the same overall complexity and same overall performance. Its main advantage is the low PAPR which is favored in mobile

terminals, but equalization is a necessity since it suffers from ISI. The three sub-carriers mappings IFDMA, LFDMA, and B-IFDMA governs the tradeoff between how much frequency diversity can be collected, how much amplifier efficiency can be achieved, and how much BER performances can be reached. IFDMA collects lots of frequency diversity, LFDMA reduces the pilot overheads to estimate the channel, and B-IFDMA combines the advantages of both. Also, IFDMA provided the lowest PAPR followed by B-IFDMA and then LFDMA in the case without pulse shaping which will be introduced in the coming chapters.

4 CHANNEL CODING, MODULATION AND PULSE SHAPING

This chapter introduces the need for channel coding to improve BER performances. Each of the Convolutional and Turbo codes will be presented showing the encoder and decoder structures. Then QPSK and 16-QAM baseband modulations will be explained, followed by pulse shaping which is a necessity to remove the out-of-band signal radiations.

4.1 Channel Coding

Channel coding is the process of adding redundant bits to the information bits to combat the errors introduced by the transmission channel. Among the channel codes, block codes, convolutional codes, and turbo codes are prominent ones and are used much in practice. In the following sections, convolutional and turbo codes, their structure, encoding and decoding process are explained.

4.1.1 Convolutional Codes

Like linear block codes, convolutional codes also map k bit input sequence to n bit codeword. Code rate $R_c = k/n$ of a code is defined as the ratio of number of input bits to the encoder to the number of output bits generated from the encoder. k is usually chosen as 1 in practice. In linear block codes, generation of output bit from an encoder just depend on the current input bit and doesn't depend on past input bits. Whereas in convolutional codes which contain memory, the present output bit of the encoder depends on the past input bits as well.

Convolutional codes are represented by generator polynomials and they are usually given in octal format. The convolutional code generator polynomials used in this thesis are of 1/2 rate and are in octal format as $[G1 \;\; G2] = [53 \;\; 75]$. In polynomial format they are represented as $G1 = 1+D^2+D^4+D^5$ and $G2 = 1+D+D^2+D^3+D^5$. Each D represents delay memory element and the highest degree of the polynomial gives the number of memory elements used in the encoder. The encoder structure for the these polynomials is shown in figure 4.1.

The contents of the shift register constitute the state of the encoder. Convolutional codes are completely described either by state diagram or trellis structure. State diagram represents the transition changes from one state to another state based on the input bit. Trellis is just a replication of the state diagram but in time and is normally used to show the decoding procedure. Because of memory elements

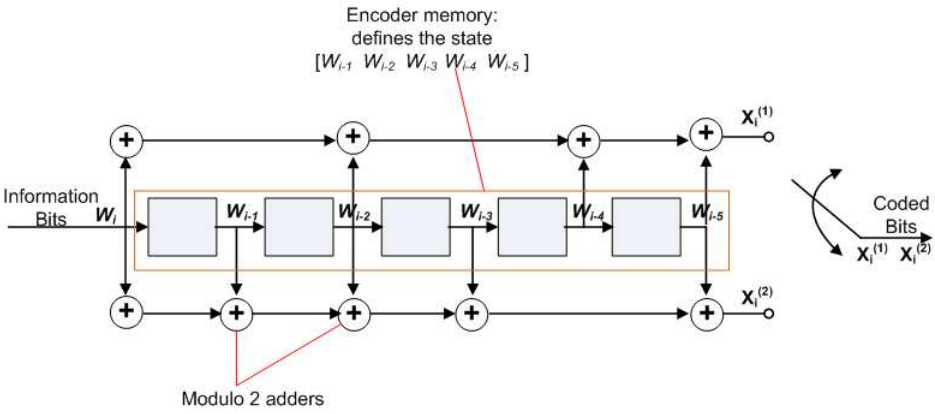

Figure 4.1. Convolutional Encoder for the Polynomial [G1 G2] = [53 75].

possessed by the convolutional encoder, it results in a finite state machine.

The dependency of output bits on past input bits is given by constraint length K. If the number of memory elements in the shift register is μ then constraint length is given as $K = \mu + 1$. So the constraint length of the convolutional encoder shown in figure 4.1 is 6. Constraint length is defined as the maximum span over which the output bit is dependent on past input bits or in other words how much the present entered bit will influence the next K output bits.

The performance of a convolutional code depends on the constraint length. Usually convolutional code with large constraint length performs better compared to codes with low constraint length. But the problem of the codes with large K is that the complexity of the viterbi decoder which is used in practice to decode convolutional codes, is exponentially proportional to the constraint length. The number of states in a trellis diagram at a particular instant of time or stage is 2^{K-1}. Each state has $2k$ branches entering and $2k$ branches leaving from it. The number of paths through the trellis grows exponentially with k, K and with length of the trellis path.

Decoding of convolutional encoded bits are done by Viterbi decoder which is based on the maximum-likelihood decoding principle. Possible paths in a trellis represents possible coded sequence. Decoding is done by finding a path that is closest to the received sequence. The operation of the viterbi decoding can be explained with the help of the block diagram in figure 4.2 (Lie Qian n.d.). The viterbi decoder consists of the following blocks.

- **BMU**: The branch metric unit (BMU) calculates the set of branch metrics for each new input symbol with the possible code symbols at each stage of the trellis diagram.
- **ACSU**: The add-compare-select unit (ACSU) accumulates the output from BMU and selects the survival paths for each input. Survival paths are obtained for each state at a particular stage of the trellis.

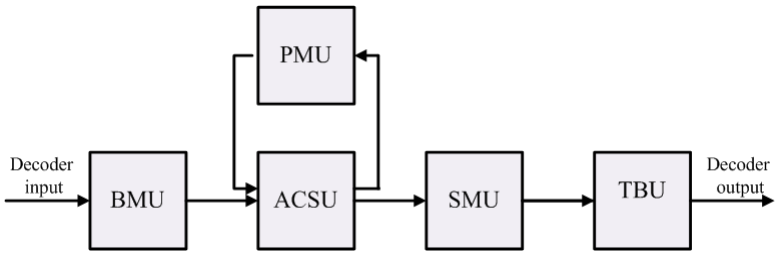

Figure 4.2. Viterbi Decoder.

- **PMU**: Accumulated value of branch metric is known as a path metric. The path metric at the present stage of trellis are obtained by adding the branch metrics of present stage of the trellis to the previous stage path metrics. The role of path memory unit (PMU) is to update and store the path metric for each survival path.

- **SMU**: The survival memory unit (SMU) stores the survival paths of all the stages of the trellis.

- **TBU**: The trace back unit (TBU) finds the state sequence, which has the minimum path metric and stores the state sequence. From the state sequence, the decoded sequence can be derived.

There are two kinds of viterbi decoding procedures based on metric calculation and are called hard decision and soft decision decoding. In hard decision decoding the output of the demodulated samples are converted to 0 or 1 before sending them to the BMU of the decoder. Received channel samples are converted to 0 or 1 based on whether the sample value is less or greater than zero. Whereas in soft decision decoding the demodulated samples are directly sent to the BMU of the decoder with out any modifications.

The procedure of hard and soft decision decoding is given in shown 4.3 (Woerner 1994). A much detailed process on viterbi decoding can be found in classical texts on error control coding especially in (Shu Lin 2004).

Hard decision decoding scheme is simpler and has comparatively less complexity than soft decision decoding. The complexity is reduced while calculating the metrics in the BMU unit. In hard decision decoding, branch metrics are calculated using hamming distance whereas in soft decision decoding, metrics are computed based on squared Euclidian distance. Hard decision decoding also saves the memory because it is easy to store bits than a floating point number as it takes more bits to represent a floating point number. But hard decision decoding suffers a performance loss of 2.5 dB compared to soft decision decoding.

Terminating trellis of convolutional encoder is of great importance. The encoder should start and end at zero state, then the decoder will know from which state to

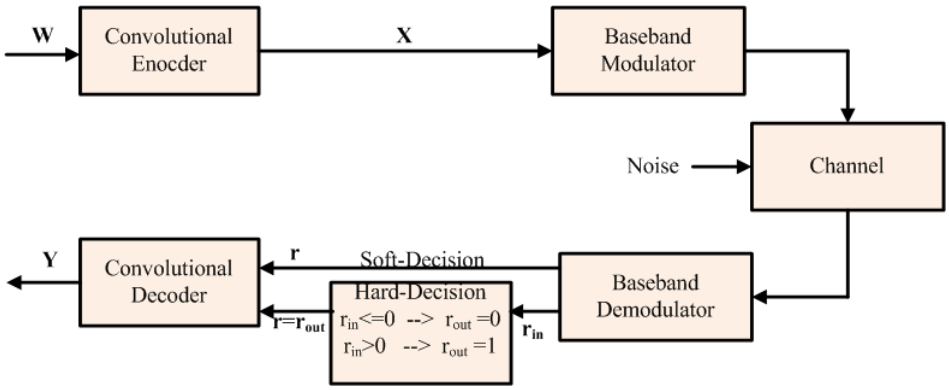

Figure 4.3. Hard and Soft Decision Decoding.

start decoding and then trace back. Encoder is terminated to zero state by flushing the shift register with zeros equal to the constraint length.

In practice there is no need to wait until the end of the whole received sequence duration and trace back to decode the bits. Observations shown in practice that at time t we can decode the information bit at time $t - t_d$ with out any significant loss of performance if $t_d \geq 5K$, since survivor paths typically merges for $t_d \geq 5K$. This saves up the processing time so that there is no need to wait until end of the whole received sequence duration to decode bits (Rodger E. Ziemer Aug 2000).

Performance of convolutional codes also depends on free distance d_{free} and distance spectrum. d_{free} for convolutional codes is the minimum hamming distance between two code sequences associated with trellis paths that diverge from one another at some point and merge at some other point. The larger the d_{free} for a set of generator polynomials, the greater is its error correcting capability. A complete survey on convolutional codes, their free distance and distance spectrum for various rates is given in (Pål Frenger and Ottosson 1999).

The rate and free distance of the convolutional code together decide the achievable coding gain. The gain in power efficiency at higher signal-to-noise ratios (SNR) is called asymptotic coding gain and is denoted by G_{coding}. The asymptotic coding gain expressed in dB for a convolutional code with code rate R_c and free distance d_{free} is given in equation 4.1. The BER performance achieved by using channel codes, is the same as the uncoded BER curve but shifted to the left by an amount equal to the asymptotic coding gain at high SNR.

$$G_{coding} = 10 \log_{10}(R_c \, d_{free}). \tag{4.1}$$

4.1.2 Turbo Codes

As in most coding techniques, having a clear structure means that the decoding can be made easier; however this doesn't ensure the best distance properties for

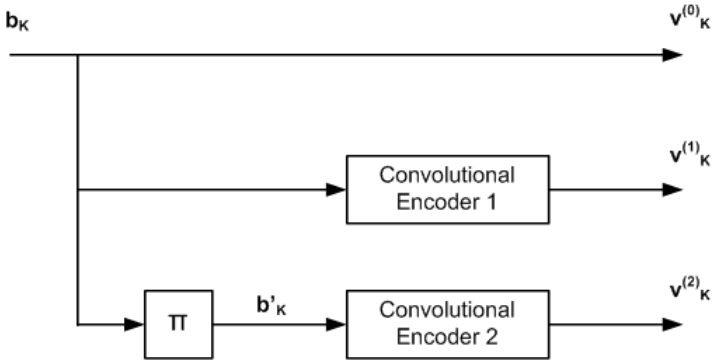

Figure 4.4. Turbo Encoder.

a code (Shu Lin 2004). Turbo codes with their parallel concatenated approach, achieves the random-like code design providing an exceptionally good performance with an enough structure to allow an efficient iterative decoding technique. In fact, very good performance can be achieved at moderate BER but for large block lengths, which in turns leads to longer decoding delays.

The block diagram of an Turbo encoder is shown in figure 4.4 where it consists of an input sequence $\mathbf{b}_K$, with two systematic feedback convolutional encoders and an interleaver.

So the first parity sequence $\mathbf{v}_K^{(0)}$ is nothing but the original information sequence $\mathbf{b}_K$. The first encoder generates the second parity sequence $\mathbf{v}_K^{(1)}$, and the last encoder encoder the permuted or reordered sequence $\mathbf{b}'_K$ to get the third parity sequence $\mathbf{v}_K^{(2)}$. The final transmitted codeword is

$$\mathbf{v}_{3K} = (v_0^{(0)} v_0^{(1)} v_0^{(2)}, v_1^{(0)} v_1^{(1)} v_1^{(2)}, \ldots, v_{K-1}^{(0)} v_{K-1}^{(1)} v_{K-1}^{(2)}).$$

The iterative turbo decoder as shown in figure 4.5 deploys two Soft-Input Soft-Output (SISO) decoders using Maximum A Posteriori (MAP) algorithm.

At each time instant t, three values are received corresponding to the original information value $r_t^{(0)}$ and the two other parity values $r_t^{(1)}$ and $r_t^{(2)}$. Together with the channel reliability factor $L_c = 4\frac{Es}{N_0}$ and the extrinsic values $L_e(b_t)$ which are the decoder outputs, form the input of these decoders. $L_c r_t^{(0)}$ and $L_c r_t^{(1)}$ together with $L_e^{(2)}(b_t)$ are passed to decoder 1 while $L_c r_t^{(0)}$ and $L_c r_t^{(2)}$ together with $L_e^{(1)}(b_t)$ are passed to decoder 2. Starting with $L_e^{(2)}(b_t) = 0$ in the case of equally likely information bits, decoder 1 operates thus passing the extrinsic value $L_e^{(1)}(b_t)$ which will be treated as a new set of a priori probabilities by the MAP algorithm of decoder 2. Same things goes with decoder 2 which outputs $L_e^{(2)}(b_t)$, where this value will be used by decoder 1 in the next iteration. Thus decoding iterates resulting in more and more reliable estimates. Finally, after a number of sufficient iterations, the a posteriori values $L^{(2)}(b_t)$ resulting from decoder 2 determines the most probable transmitted information bits.

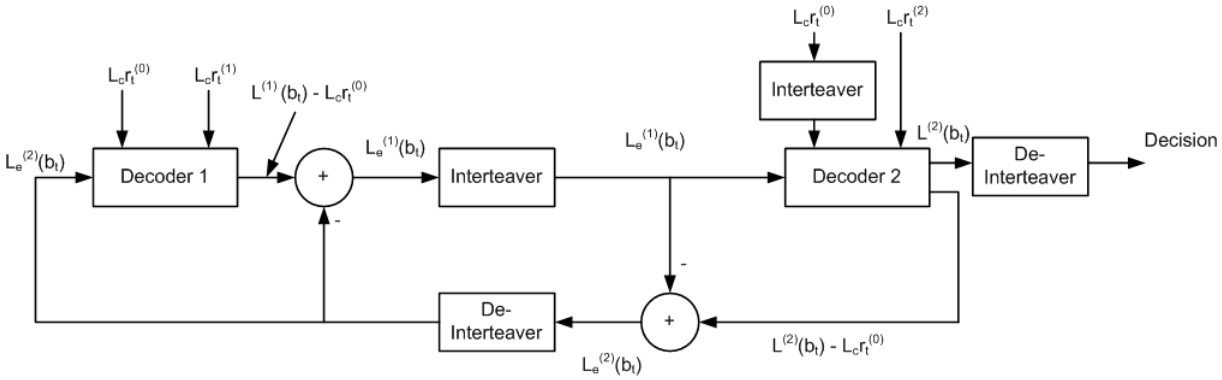

Figure 4.5. Iterative Turbo Decoder.

4.2 Baseband Modulation

In this section, a very brief description about digital modulation techniques that were used in this thesis were given. These are the Quadrature Phase Shift Keying(QPSK) and Quadrature Amplitude Modulation (QAM), where each maps a different number of bits to symbols.

Firstly about QPSK, as the name suggests in this modulation technique the information is carried on the phase. It consists of 4 points in the constellation diagram corresponding to four different phases as in figure 4.6. All the constellation points are equally spaced on a circle and have unit symbol energy. Sometimes this modulation scheme is also referred to as 4-PSK, suggesting that its PSK scheme with four constellation points and as 4-QAM since it also forms a rectangular constellation.

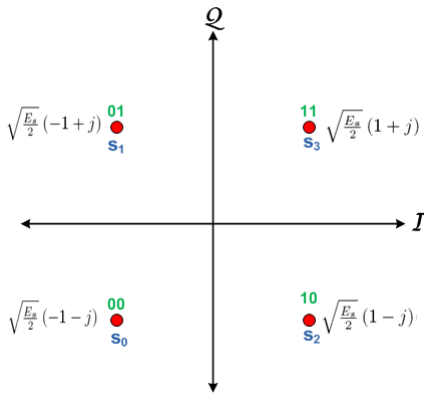

Figure 4.6. QPSK Constellation.

In the case of QPSK, it maps 2 bits to a symbol, and the bit to symbol mapping is also depicted in figure 4.6. Usually Gray coding is used so the bits corresponding

to two neighboring symbols differ in only one position. This is very helpful in noisy channel as symbols errors leads to few bit errors.

The probability of bit error P_b of QPSK in AWGN channel is same as in the case of BPSK and is given in equation 4.2.

$$P_b = Q\left(\sqrt{\frac{2E_b}{N_0}}\right) \tag{4.2}$$

where E_b is the energy per bit, N_o is the noise power spectral density and Q is Q-function.

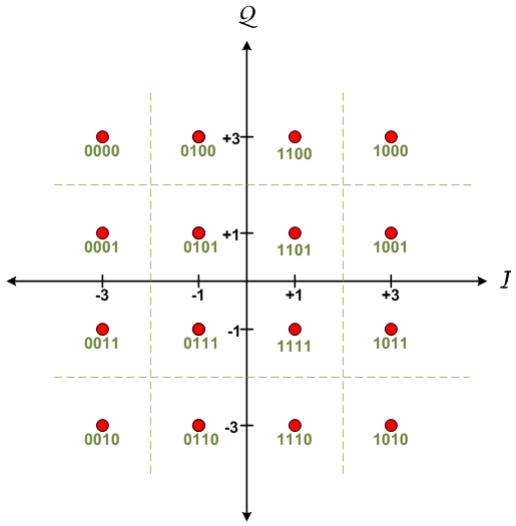

Figure 4.7. 16-QAM Constellation.

Unlike QPSK, 16-QAM has a rectangular constellation points shown in figure 4.7. In 16-QAM each symbol comprises of 4 information bits and information is carried on phase and amplitude . Since the constellation is rectangular with multilevels, all the symbols don't have equal symbol energy. In this case also the Gray coding has been used for bit to symbol mapping to reduce bit errors. The bit error performance is very low compared to QPSK because of its tight decision boundaries as depicted in figure 4.7. The probability of bit error P_b of 16-QAM is given in equation 4.3.

$$P_b = \frac{3}{2k}\, erfc\left(\sqrt{\frac{kE_b}{10N_o}}\right), \tag{4.3}$$

where E_b is the energy per bit, N_o is the noise power spectral density, *erfc* is complimentary error function and $k = 4$ is the number of bits per symbol . Uncoded theoretical bit error probability for QPSK and 16-QAM in AWGN channel is shown in figure 4.8. From the figure, it can be observed that at high SNR, 16-QAM suffers a performance degradation of 4dB compared to QPSK. On the other hand, 16-QAM has twice as much as the data rate of QPSK.

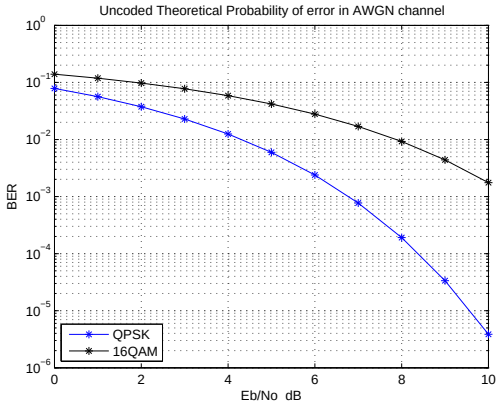

Figure 4.8. Uncoded Theoretical Probability of Error for QPSK and 16-QAM in AWGN Channel.

4.3 Pulse Shaping

Bandwidth is a scarce resource obliging data transmission systems to constrain the bandwith of their transmitted signals. But the drawback is the increase in the likelihood of decoding errors (Gentile 2007). Pulse-shaping is a technique used to restrict the bandwidth of the transmitted signals while minimizing the likelihood of decoding errors.

To better clarify the importance and the mechanism behind pulse-shaping, one should examine the most basic information unit in digital transmission, and the same concept will be valid on more sophisticated systems. Starting with the time domain representation of a rectangular pulse as shown in figure 4.9, we can see that the spectrum or frequency domain representation is nothing but the *sinc* response where the null points occur at integer multiples of f_0 which is the pulse rate. In theory, the spectrum of a rectangular pulse is infinite but in this figure, the spectrum from $-5f_0$ to $+5f_0$ is shown.

This infinite bandwidth associated with the rectangular pulse can be limited by applying a low-pass filter. The well know pulse-shaping filter is known as the raised cosine filter with its frequency response as defined in equation 4.4 and impulse response in equation 4.5.

$$H_{RC}(f) = \begin{cases} \tau, & |f| < \frac{1-\alpha}{2\tau}; \\ \frac{\tau}{2}\left[1 + cos\left(\frac{\pi\tau}{\alpha}\left(|f| - \frac{1-\alpha}{2\tau}\right)\right)\right], & \frac{1-\alpha}{2\tau} \leq |f| \leq \frac{1+\alpha}{2\tau}; \\ 0, & \text{otherwise;} \end{cases} \tag{4.4}$$

where f is the frequency, τ is the pulse period, and α is the roll off factor.

$$h_{RC}(t) = sinc\left(\frac{t}{\tau}\right)\left[\frac{cos\left(\frac{\pi\alpha t}{\tau}\right)}{1 - \left(\frac{2\alpha t}{\tau}\right)^2}\right], \tag{4.5}$$

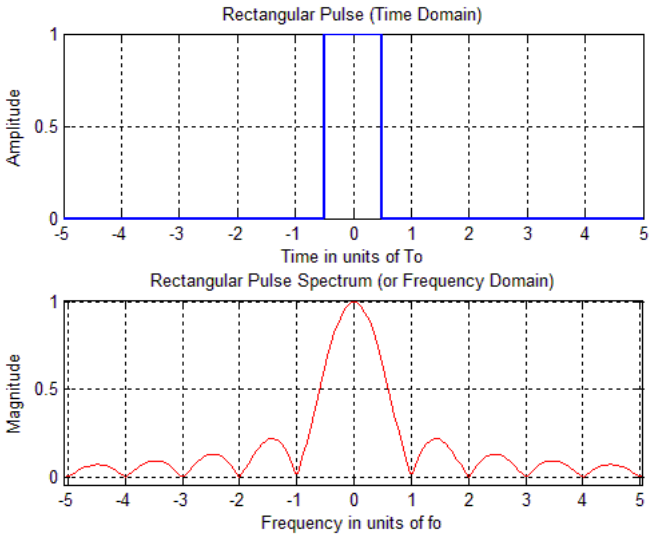

Figure 4.9. Rectangular Pulse Time and Frequency Domain Representation.

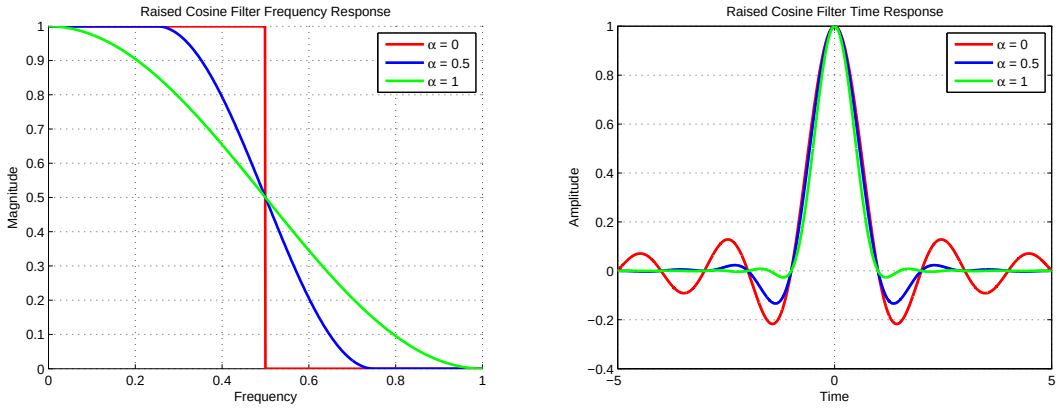

Figure 4.10. Frequency and Time of RC Filter.

where t is the time.

Based on the roll-off factor, the response characteristics of the raised cosine filter will change, and this will be reflected in the different oscillations observed in the impulse response (time domain) as presented in figure 4.10.

Oscillations in the impulse response are the consequence of limiting the filter bandwidth to a value less than infinity. The tighter the bandwidth in the frequency domain, the higher the side lobes in the time domain. Figure 4.11 shows the resulting time domain rectangular pulse after pulse shaping which turns out to be a smoothly rounded pulse with ripples before and after the original period τ where the ripples' amplitude reflect what roll-off factor was used.

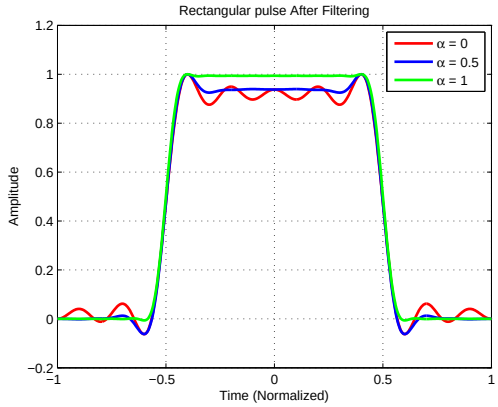

Figure 4.11. Rectangular Pulse after Pulse Shaping.

The key property of the RC filter is that the zero crossings of the impulse response coincides with the midpoint of the consecutive pulses (Gentile 2007). So if the receiver is capable of sampling exactly at the midpoints of the pulses, then no errors result regardless of the roll-off factor used since each sampling point doesn't contain information from adjacent pulses. But in reality, this is not the case and this will lead to intersymbol interference (ISI) which increases the likelihood of decoding errors. So the trade-off between the bandwidth containment in the frequency domain and the ripple attenuation in the time domain (causing ISI) should be considered while designing communication systems (Gentile 2007).

5 SYSTEM SIMULATION AND DISCUSSION

This chapter will deal with defining the system model of the uplink multiple access scheme of IMT-Advanced, setting the parameters used in the simulations. PAPR analyses, in addition to BER performances will be presented, analyzed, and conclusions will be drawn highlighting the optimal parameters.

5.1 System Model

In this section, the system model for DFT-precoded (IFDMA, LFDMA, B-IFDMA), and non DFT-precoded (B-EFDMA) techniques will be derived for a single user. Discrete time representation of all the signals will be used with the following notations: $(.)^T$ as the transpose, $(.)^{-1}$ as the inverse, $(.)^\dagger$ as the pseudo inverse, and $(.)^H$ as the Hermitian.

Throughout the derivations, a system with Q users will be used with user index q where $q = 0, 1, \ldots, Q-1$ and raw data for each user denoted as $\mathbf{d}^{(q)}$. The block diagram with the corresponding matrix representation for each block is shown in figure 5.1. The raw data is firstly processed by the channel encoder block using Convolutional or Turbo coding. The coded bits in one chunk duration are then randomly interleaved, where a chunk is a time-frequency unit where the subcarriers included experiences flat fading, and the interleaver depth is affected by the size of the chunk. This is followed by baseband modulation (QPSK or 16-QAM) where normalization is applied to keep the energy of the modulated symbols as unity. So the modulated symbols in one OFDMA/SC-FDMA symbol is denoted as $\mathbf{s}_K^{(q)} = (s_0^{(q)}, \ldots, s_k^{(q)}, \ldots, s_{K-1}^{(q)})^T$, where K is the number of subcarriers allocated to a user. The data rate achieved for a particular user is directly dependent on K.

In the case of non DFT-precoded OFDMA, the modulated symbols are considered as frequency symbols and mapped on the available subcarriers allocated to a user. These are then transmitted over the channel by applying IFFT, and then corrupted by AWGN. So the received symbol in a non DFT-precoded OFDMA system can be expressed as a vector of length M samples (i.e. total number of subcarriers in the system where $M = Q.K$) defined as:

$$\mathbf{r}_M^{(q)} = \mathbf{H}^{(q)} \,.\, \mathbf{F}_M^H \,.\, \mathbf{T}^{(q)} \,.\, \mathbf{s}_K^{(q)} \; + \; \mathbf{w}_M, \tag{5.1}$$

where $\mathbf{T}$ is the subcarrier mapping matrix which is user dependent, $\mathbf{F}_M^H$ is the matrix representation of the Inverse Fast Fourier Transform (IFFT), $\mathbf{H}^{(q)}$ is the multipath propagation channel coefficient matrix of the WINNER C2 NLOS for the q^{th} user (Baum *et al.* Nov. 2005) , and $\mathbf{w}_M$ is the Additive White Gaussian Noise (AWGN).

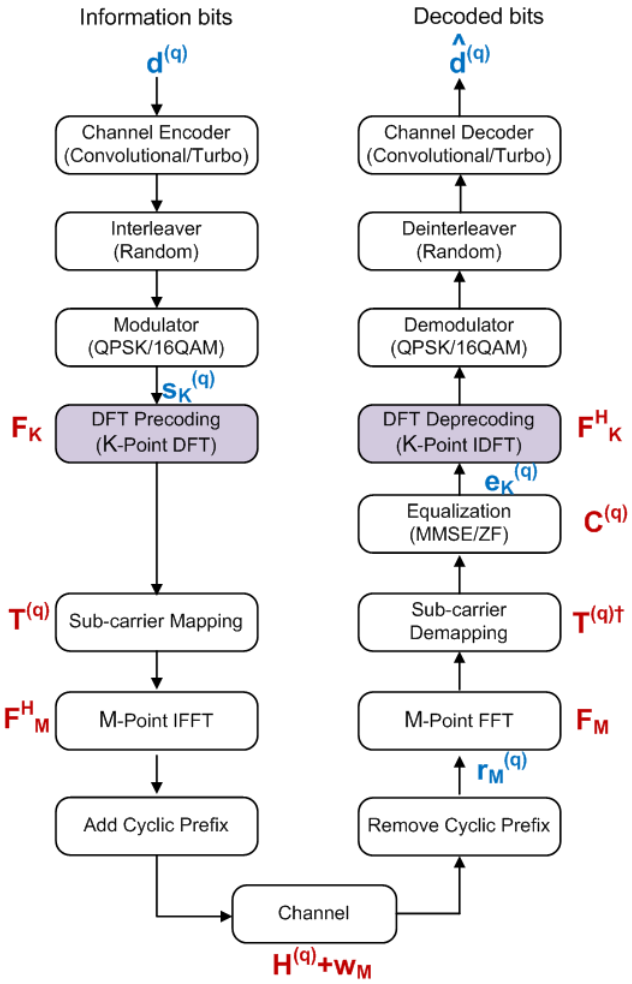

Figure 5.1. IMT-Advanced Uplink System Model.

The cyclic prefix is not included in the equation since it is an addition and removal of some redundant bits to eliminate the ISI but has no effect on the mathematical modeling of the overall system as long as its length is at least equal to the maximum delay spread of the channel.

The only difference between non DFT-precoded OFDMA and DFT-precoded OFDMA scheme is the presence of the DFT-precoding block which is shaded in the block diagram. In other words, the modulated symbols are DFT-precoded resulting in the frequency domain symbols, and the same procedure is followed as the non DFT-precoded case. The mathematical representation of the received signal will be:

$$\mathbf{r}_M^{(q)} = \mathbf{H}^{(q)} \,.\, \mathbf{F}_M^H \,.\, \mathbf{T}^{(q)} \,.\, \mathbf{F}_K \,.\, \mathbf{s}_K^{(q)} \;+\; \mathbf{w}_M, \tag{5.2}$$

To compensate the impact of the channel, equalization is applied and the equalized

received samples can be expressed as a vector of length K expressed as

$$\mathbf{e}_K^{(q)} = \mathbf{C}^{(q)} \,.\, \mathbf{T}^{(q)\dagger} \,.\, \mathbf{F}_M \,.\, \mathbf{r}_M^{(q)}, \tag{5.3}$$

where $\mathbf{F}_M$ represents the M-point Fast Fourier Transform (FFT), $\mathbf{T}^{(q)\dagger}$ is the subcarrier demapping matrix, $\mathbf{C}$ is the equalization matrix. Note that Zero Forcing (ZF) equalization and Minimum Mean Square Error (MMSE) Equalization are the two Frequency Domain Equalizers (FDE) that were used in this system and which are defined as:

$$\mathbf{C}_{ZF} = \frac{1}{\mathbf{H}}, \tag{5.4}$$

and

$$\mathbf{C}_{MMSE} = \frac{\mathbf{H}^H}{|\mathbf{H}|^2 + \frac{\sigma_w^2}{\sigma_s^2}}, \tag{5.5}$$

where σ_w^2 is the variance of the AWGN, and σ_s^2 is the variance of the modulated symbols.

In the case of non DFT-precoded OFDMA/SC-FDMA, the equalized samples are then demodulated, deinterleaved and decoded to get the estimated transmitted data block $\hat{\mathbf{d}}^{(q)}$. Whereas in the case of DFT-precoded OFDMA/SC-FDMA, the above mentioned steps are preceded by a DFT-predecoder.

The difference between the subcarrier mapping schemes is nothing but how the K symbols corresponding to one user are mapped on to one OFDMA/SC-FDMA symbol which has a length equal to the total number of subcarriers in the system.

The subcarrier allocation matrix (T) of size $M \times K$ can be represented by the following:

- *IFDMA*

$$T_{IFDMA}^{(q)}(m,k) = \begin{cases} 1, & m = k.Q + q; \\ 0, & \text{otherwise}; \end{cases} \tag{5.6}$$

- *LFDMA*

$$T_{LFDMA}^{(q)}(m,k) = \begin{cases} 1, & m = q.K + k; \\ 0, & \text{otherwise}; \end{cases} \tag{5.7}$$

- *B-IFDMA* and *B-EFDMA*

$$T_{B-IFDMA}^{(q)}(m,k) = T_{B-EFDMA}^{(q)}(m,k) = \begin{cases} 1, & m = p.\frac{M}{P} + l + q.L; \\ 0, & \text{otherwise}; \end{cases} \tag{5.8}$$

where P denotes the number of blocks assigned to a specific user, $p = 0, \ldots, P-1$ is the index of the blocks. L is the number of subcarriers in each block where $l = 0, \ldots, L-1$ is the subcarrier index in a particular block.

Bandwidth	80 MHz
Carrier Frequency (Fc)	3.7 GHz
Sampling Time (Ts)	12.5 ns
Sampling Rate (Fs)	1/(12.5 ns)
Guard Interval	1.47 μs
Total Number of Subcarriers (M)	1024
Number of Subcarriers per User (K)	64, 128
Subcarriers per Block (L)	2, 4 ,8, 16
Chunk Width (Nt)	4,8,12
Modulation	QPSK, 16-QAM
Coding	Convolutional code, rate=1/2, G1= $1 + D^2 + D^4 + D^5$, G2= $1 + D + D^2 + D^3 + D^5$, Constraint length=6, Soft Input Viterbi Decoder
	Turbo code, rate=1/2 [G1,G2]=$[1 + D + D^2 + D^3 + D^4; 1 + D^4]$, Constraint length=5, LogMAP Decoder
Interleaver	Random
Equalizer	MMSE FDE ZF FDE
Channel	WINNER C2 NLOS User velocity = 50 Km/h Coherence Bandwidth=680.27 KHz Coherence Time(=$1/f_D$) = 5.8 ms
Channel Estimation	Perfect CSIR Estimated CSIR using Wiener filter

Table 5.1. Simulation Parameters.

5.2 Simulations

A series of simulations have been performed taking into consideration the different system parameters presented in table 5.1. Simulations include performance comparisons of the different aforementioned mapping schemes with different modulation techniques, equalization methods, channel coding, and channel estimation, all tested

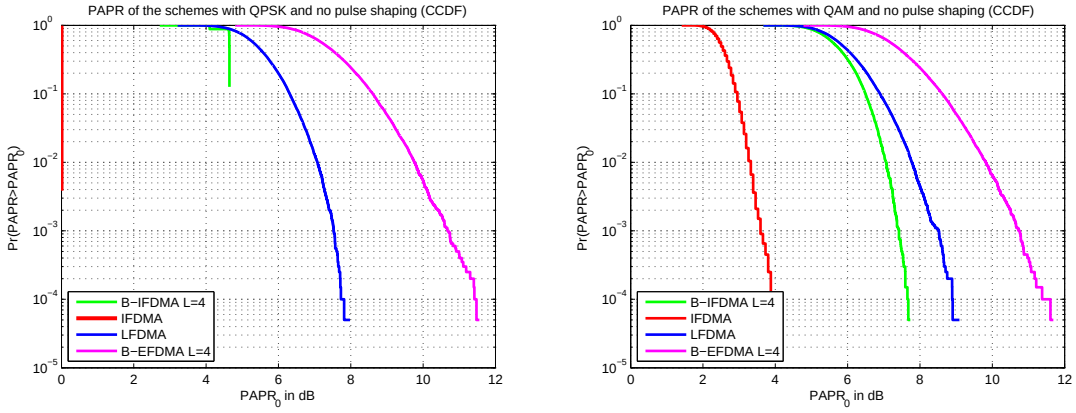

Figure 5.2. PAPR of IFDMA, B-IFDMA, LFDMA, and B-EFDMA with QPSK (Left) and 16-QAM (Right) but without Pulse Shaping.

under Rayleigh fading channel with WINNER C2 NLOS power delay profile in the presence of AWGN which models the receiver's noise. Moreover, all the simulations were carried out under the same data rate in order to have a fair comparison.

Performances for the different simulations were scrutinized thus highlighting the trade off between how much frequency diversity can be collected, amplifier efficiency can be reached, and performances can be achieved in the absence of perfect channel information.

All the below simulations were performed at a data rate of 8.9667 Mbps meaning that users are allocated 128 subcarriers in the case of QPSK modulation and 64 subcarriers in the case of 16-QAM with 1/2 rate channel coding.

5.2.1 PAPR Analysis

PAPR simulations were done to figure out how much amplifiers need to backoff for the different multiple access schemes with QPSK and 16-QAM modulation.

Figure 5.2 shows the different schemes in the absence of pulse shaping. In the case of QPSK modulation (figure 5.2 left), DFT-precoding schemes had lower PAPR compared to the non DFT-precoding ones and that is because the time domain signal of the latter is the superposition of all the subcarriers with different carrier frequencies thus high amplitude peaks are inevitable. For the DFT-precoded schemes, IFDMA has the lowest PAPR followed by B-IFDMA and then LFDMA. In Section 3.2.2, the time domain representation of IFDMA shows that the transmitted signal is nothing but Q repetitions of the original signal scaled by a factor of $\frac{1}{Q}$, where Q is the number of users in the system and this explains the reason behind having the lowest PAPR. On the other hand, LFDMA has the highest PAPR since the time domain signals has the exact scaled copies of the the input signal, and with other complex

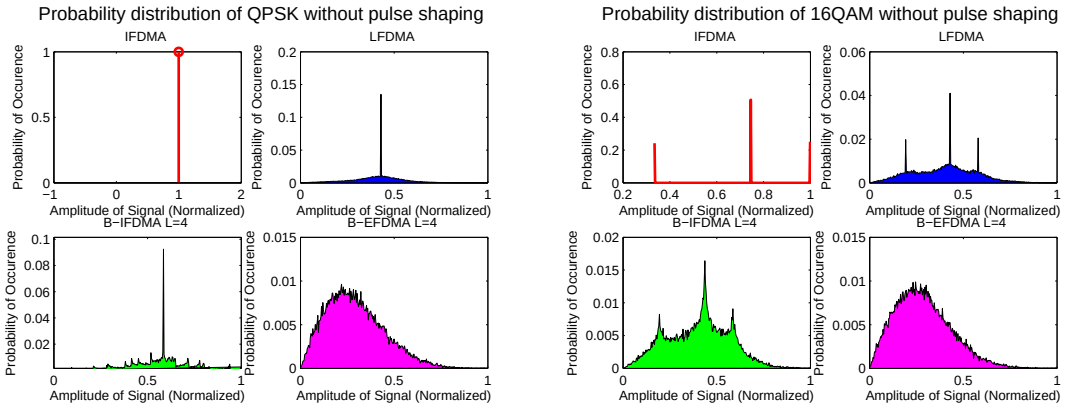

Figure 5.3. PDF of Signal Amplitude of IFDMA, B-IFDMA, LFDMA, and B-EFDMA with QPSK (Left) and 16-QAM (Right) but without Pulse Shaping.

valued signals in between, thus resulting in more variations in the amplitude. Finally, B-IFDMA falls in between the lowest PAPR IFDMA and the highest PAPR LFDMA. The main trend in the DFT-precoded schemes is that high PAPR are associated with larger block sizes. Figure 5.2 (right) shows the PAPR results for the higher order modulation 16-QAM. Same conclusion holds as that of QPSK, but a larger back-off in the high power amplifier is needed in the DFT-precoded case. On the other hand, the non DFT-precoded system is more robust to using higher order constellations although it has still the highest PAPR.

The reason why 16-QAM deteriorates the PAPR performances compared to QPSK is because the 16-QAM symbols doesn't have a constant amplitude (or energy) as in the case of QPSK where the symbols lies on a circle as shown in section 4.2.

The probability distribution of the amplitudes in figure 5.3 elicits why DFT-precoded schemes experienced more PAPR deterioration compared to the non DFT-precoded scheme when deploying a higher order modulation. It can be observed in the case of B-EFDMA that the PDF has not changed a lot reflecting a negligible drift in the PAPR Complementary Cumulative Distribution Function (CCDF) plot.

In the presence of pulse shaping, the PAPR for the different modulation and multiple access schemes increased as shown in figure 5.4. The roll-off factor governs the trade-off between the bandwidth containment and the PAPR value. For the case of DFT-precoding, increasing the roll-off factor, lowers spectral efficiency by increasing the bandwidth of symbols, but decreases the PAPR. This is explained in section 4.3 where bigger roll-off results in lower sidelobes in the time domain signal. It can be noticed that IFDMA is the most sensitive to varying the roll-off factor unlike LFDMA which is more robust and the change is negligible when different roll-off factors.

The robustness of LFDMA can be explained by the PDF in figure 5.5 where there is not much variation between the two roll-off factors. Whereas, in the non DFT-

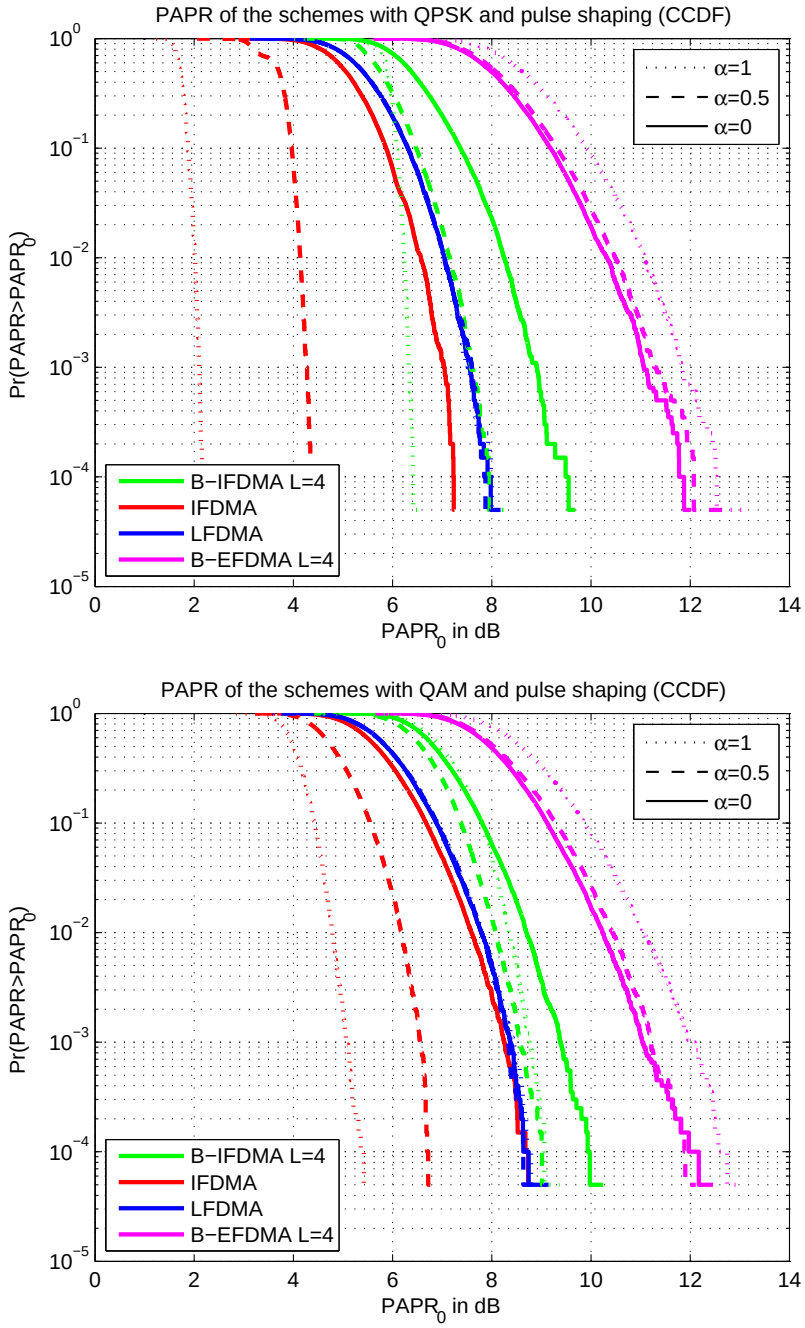

Figure 5.4. PAPR of IFDMA, B-IFDMA, LFDMA, and B-EFDMA with QPSK and 16-QAM with Pulse Shaping.

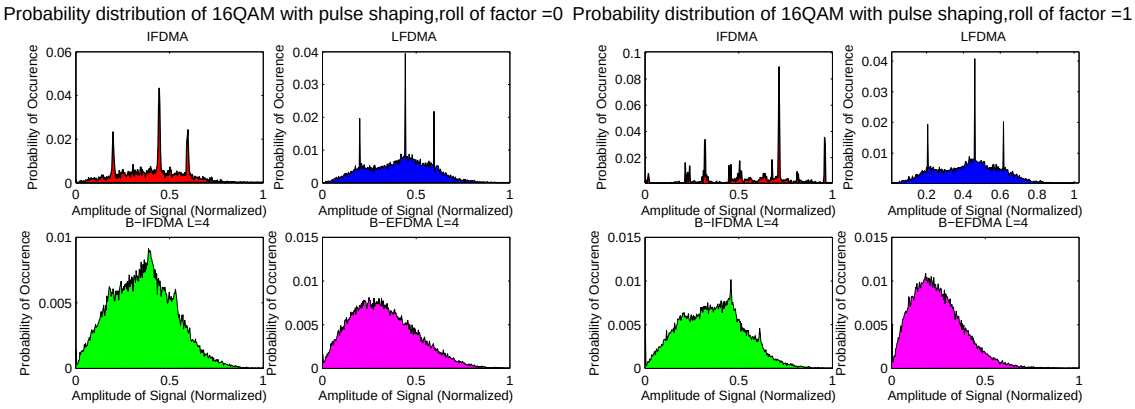

Figure 5.5. PDF of Signal Amplitudes of IFDMA, B-IFDMA, LFDMA, and B-EFDMA with 16-QAM with $\alpha = 0$(Left) and $\alpha = 1$(Right).

precoded system, reducing the roll-off factor is better although the time domain sidelobes are higher. This can also be observed in the PDF as it has been broadened thus increasing the mean of the signal amplitudes which results in less PAPR. The reason for that can be explained by looking at the frequency domain of the non DFT-precoded schemes where the subcarriers are nothing but the overlapped orthogonal sinc pulses. So filtering the OFDMA symbol in the frequency domain using the pulse shaping filter with the least roll-off factor, removes the high frequency components which causes the rapid amplitude fluctuation in the time domain. Whereas, if the roll-off factor is more, less high frequency components are removed, which leads to higher signal amplitude fluctuations thus high PAPR.

5.2.2 BER Performances

In this section, BER performances of all the schemes will be presented using QPSK first and then 16-QAM in the presence of convolutional codes. For each of the modulation schemes, there will be a comparison of results for the different equalization techniques used and the effect of interleaving will be examined followed by an analysis of the depth of the interleaver used. Then the results for the different block sizes in the case of B-IFDMA and B-EFDMA will be studied. This will be followed by showing the BER performances for specific cases where we have imperfect CSIR.

Then the two modulation schemes will be compared against each other. And finally, the BER performances with the presence of the robust Turbo codes will be examined for the cases of B-IFDMA and B-EFDMA. The effect of collecting more frequency diversity will be studies under these settings.

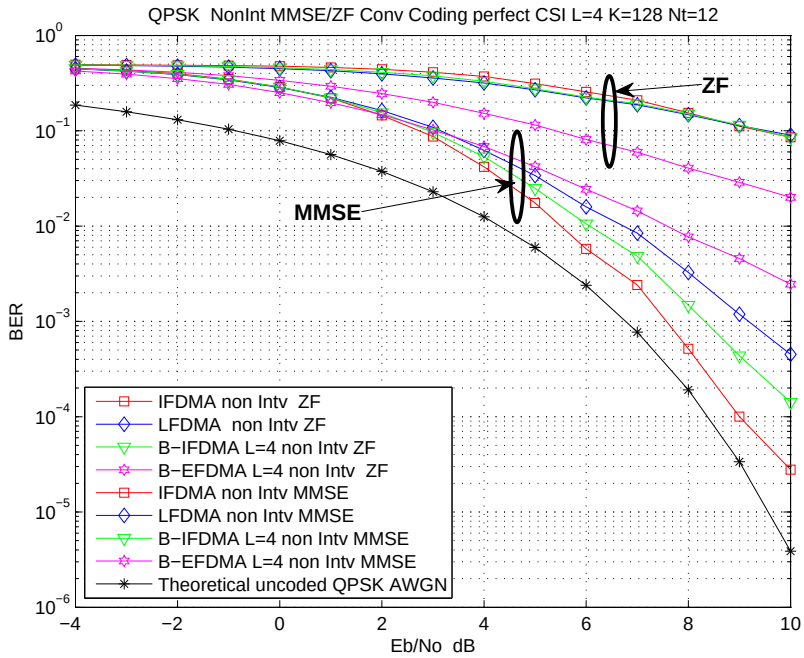

Figure 5.6. QPSK NonIntv with MMSE and ZF with Convolutional Coding and Perfect Channel Knowledge.

QPSK BER Analysis

Figure 5.6 shows the ability of MMSE to take into consideration the effect of noise while equalizing thus beating the same system equipped with ZF equalizer.

For the ZF case, non DFT-precoding performs better than the DFT-precoded case. A reason for that is because DFT-precoding introduces ISI in which the ZF equalizer is not able to mitigate its effect. Also, decreasing the block size leads to better performance after a threshold of 7 dB for B-EFDMA. This can be also observed in figure B.1. Moreover, for the DFT-precoding case, LFDMA performs the best followed by B-IFDMA and then IFDMA up till 10 dB and viceversa after SNR of 10 dB. This simply means that decreasing the block improves performance after 10 dB and this is depicted in figure 5.7 (top).

For the MMSE case, the DFT-precoded system has a better performance than the non DFT-precoded case, and decreasing the block size in both cases improves performance after an SNR of 2 dB. This is also shown in figure B.2 where B-IFDMA and B-EFDMA were simulated while varying the block sizes.

To analyze the effect of interleaver, figure 5.7 shows the simulations with and without interleaving with the use of ZF and MMSE equalizers. With the use of ZF, interleaver improves the performance of the non DFT-precoded case after an SNR of 6 dB, and the reason for that is because we end up with less error events allowing

the interleaver to provide diversity gain. Whereas, for the DFT-precoded case, up till the simulated SNRs, the interleaver worsens the performance, but it should provide with diversity gain at higher SNRs. Whereas with the use of MMSE, interleaver is better after an SNR of 3 dB for both DFT and non DFT-precoded cases with more gain in the non DFT-precoded case (B-EFDMA). For both interleaved cases, reducing the block size leads to a better performance at high SNR and this is shown in figures B.3 and B.4 but that is not so clear in the case of DFT-precoding with ZF.

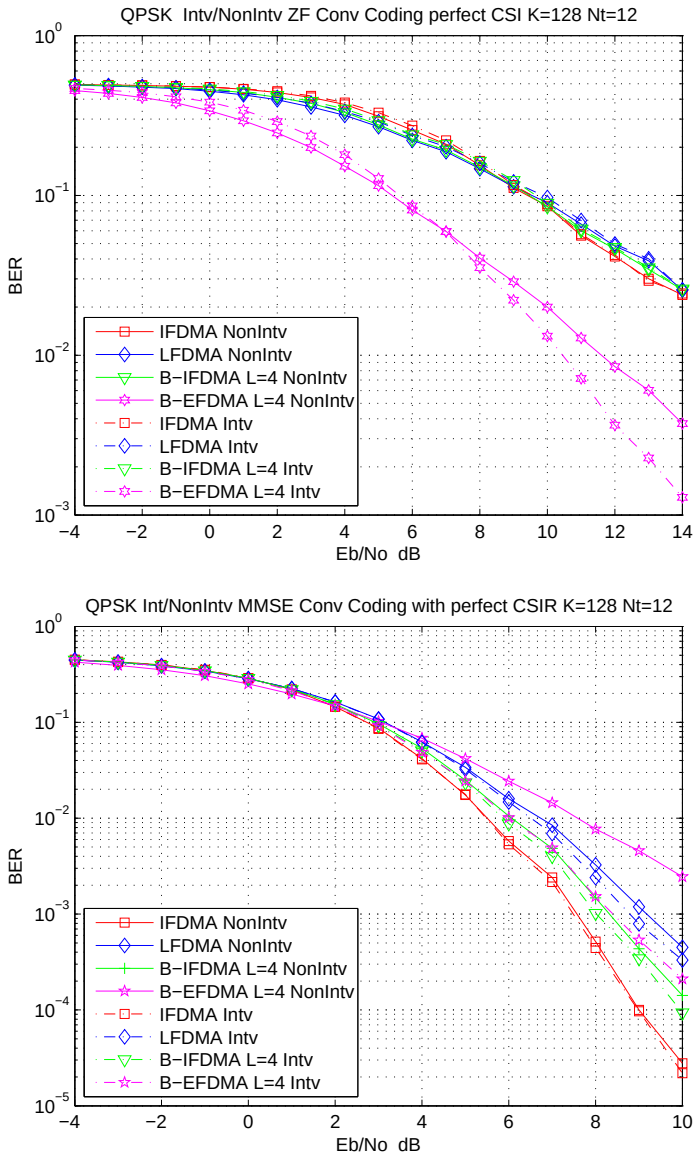

Figure 5.7. QPSK Intv/NonIntv with ZF and MMSE, Convolutional Coding, and Perfect Channel Knowledge.

Surprisingly, the size of the interleaver depth is not of a great influence on the performance in the case of having same data rate (i.e., increasing the number

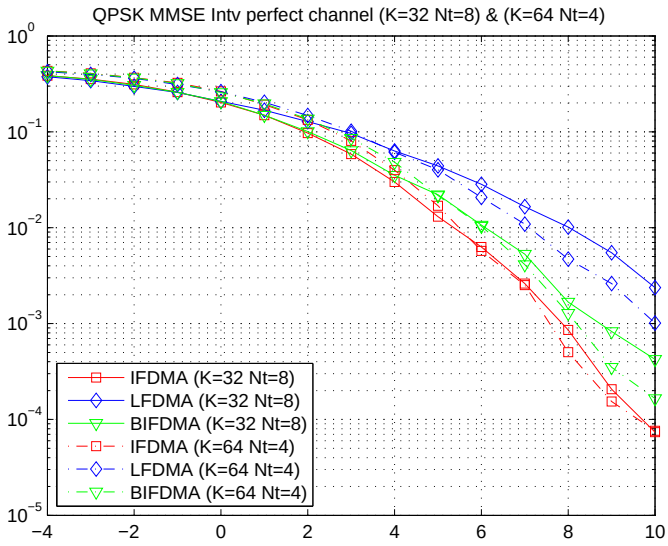

Figure 5.8. QPSK with MMSE, Convolutional Coding and perfect Channel Knowledge While Varying the Chunk Size.

of OFDMA/SC-FDMA symbols in one chunk while keeping the same number of subcarriers per symbol). Figure B.5 and B.6 explains this by showing the system with QPSK modulation, and ZF/MMSE equalization while varying the number of OFDMA/SC-FDMA symbols in one chunk (i.e., from 3 OFDMA/SC-FDMA symbols in one chunk to 12 OFDMA/SC-FDMA symbols in one chunk).

On the other hand, figure 5.8 shows that the effect of frequency diversity on the performance is more than that of time diversity (larger interleaver in time but less number of subcarriers per OFDMA/SC-FDMA symbol).

The story changes when there is a lack of receiver's channel state information as shown in figure 5.9 in the interleaved case with MMSE equalization. Using the performance degradation values due to imperfect channel estimation at the receiver presented in (Aronsson *et al.* 2009) for chunk-based Wiener filtering, LFDMA performance which was the worst in the presence of perfect CSIR, approaches B-IFDMA and B-EFDMA up till an SNR of 6 dB. The reason for that is because LFDMA allows interpolation in the frequency domain, which leads to a better channel estimation performance. For the IFDMA scheme which is performing the best in the case of perfect CSIR, it has now the worst BER performance since interpolation is rather impossible leading to a poor channel estimation performance. After an SNR of 6 dB, it can be noticed that regardless of the good channel estimation performance that LFDMA offers, collecting more frequency diversity is of a greater importance. As a result, B-IFDMA which combines the advantages of collecting frequency diversity and having a decent channel estimation performance, beats all the other schemes. Asymptotically, IFDMA will perform better due to its larger frequency diversity collection ability.

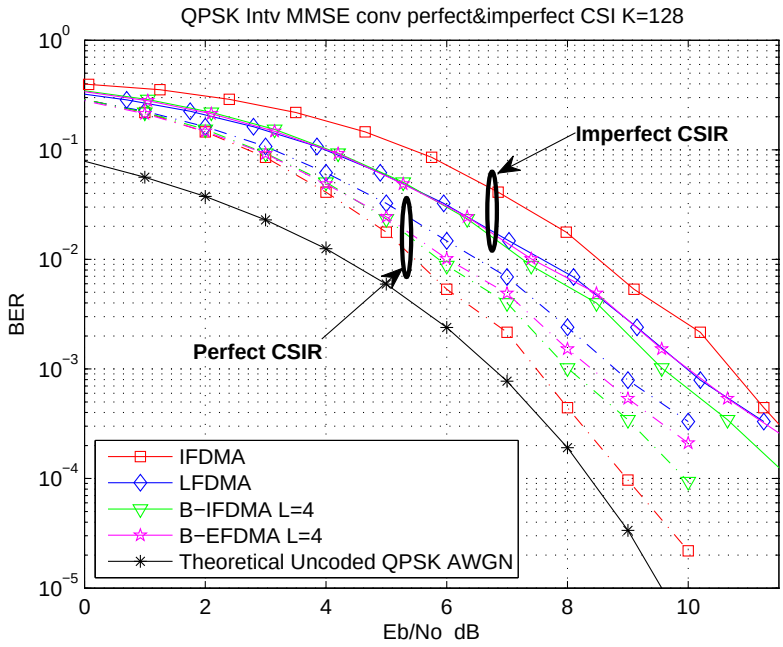

Figure 5.9. QPSK with MMSE, Convolutional Coding, Interleaver under Perfect and Imperfect Channel Knowledge.

16-QAM BER Analysis

With the QPSK modulation, MMSE equalizers provided a better performance compared to the schemes equipped with ZF, but this is not anymore valid for B-EFDMA, since with ZF, it performs better than the DFT-precoded schemes with MMSE and close to B-EFDMA with MMSE up till 8 dB. This could be related to the tight decision boundaries of 16-QAM and the fact that MMSE wasn't able to mitigate the effect of ISI introduced by the DFT-precoding.

For the ZF case, figure 5.10 shows that non DFT-precoding performs better as in the QPSK case. Up till the simulated 10 dB, increasing the block size improves the performance of DFT and non DFT-precoded cases. This is also shown in figure B.7. But at much higher SNRs, the same trend with QPSK should be noticed meaning that decreasing the block size leads to a better performance.

For the MMSE case, figure 5.10 shows that non DFT-precoding performs better as in the QPSK case but up till 8 dB, and after a threshold of 7 dB, decreasing the block size starts to lead to a better performance. This is also highlighted in figure B.8. The same figure shows that the same threshold of 7 dB holds for the DFT case, but performance results are clearly visible.

Figures 5.11 and 5.12, shows the effect of interleaving in the presence of ZF and MMSE equalizers respectively. In the ZF case, same conclusion for QPSK holds, where interleaving worsens the performance for the DFT-precoding case, and leads

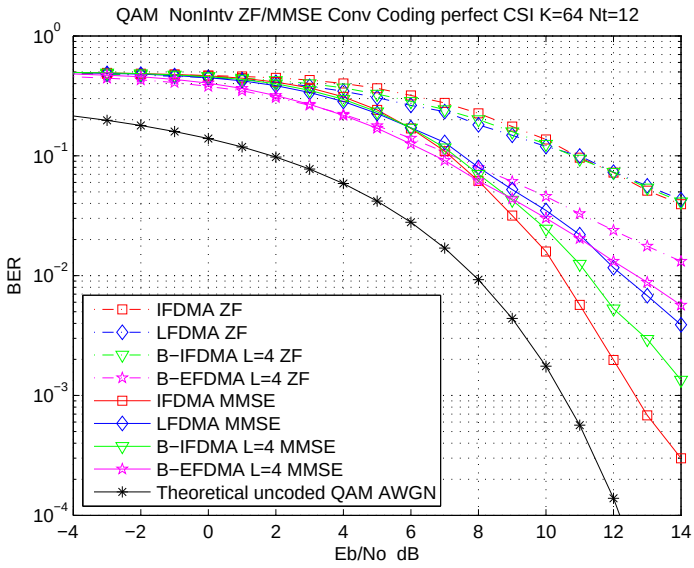

Figure 5.10. 16-QAM NonIntv with MMSE and ZF with Convolutional Coding and Perfect Channel Knowledge.

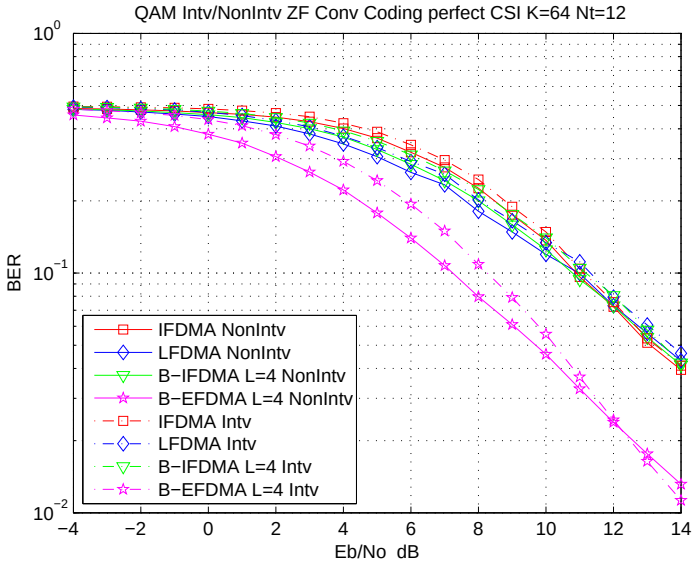

Figure 5.11. 16-QAM Intv NonIntv with ZF, Convolutional Coding and Perfect Channel Knowledge.

to better performance for the non DFT-precoding case after a threshold of 12 dB. For the MMSE case, like with QPSK modulation, interleaving improved the performance but after an SNR of 8 dB.

For the interleaved ZF case, in figure 5.11 and B.9 shows that varying block size does

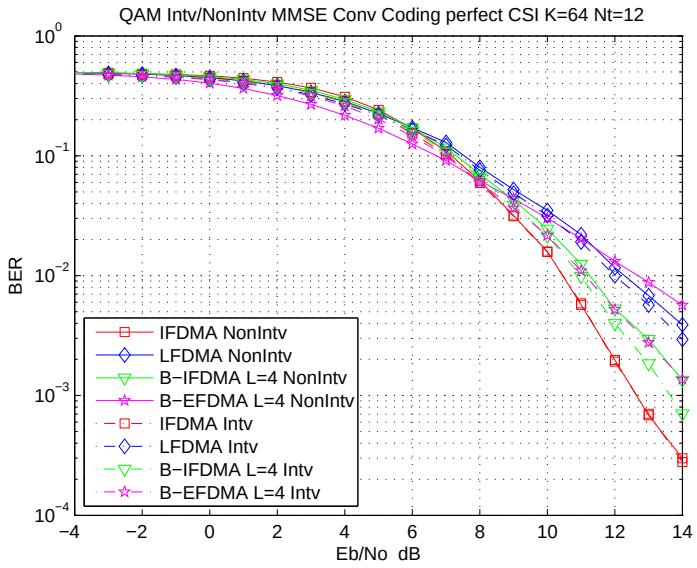

Figure 5.12. 16-QAM Intv NonIntv with MMSE, Convolutional Coding and Perfect Channel Knowledge.

not have a significant impact on the performance in the non DFT-precoding case, whereas decreasing the block size leads to improved performance after a threshold of 12 dB for the DFT-precoded case. On the other hand, decreasing the block size lead to enhanced performance for the DFT as well as non DFT-precoded cases as in figure B.10. Regarding the variation of the depth of the interleaver, same conclusion holds as in the case with the QPSK modulation.

As show in figure 5.13, IFDMA has the best performance followed by B-IFDMA, B-EFDMA and then LFDMA at high SNR under perfect channel knowledge. But under imperfect CSIR, and using the Wiener filter estimation, the same conclusion holds as in the case with QPSK modulation but B-EFDMA approaches B-IFDMA. The possible reason for that is the tight decision boundaries in 16-QAM and the ISI introduced by DFT-precoding.

QPSK vs 16-QAM

Figure 5.14 shows the performance with interleaving and MMSE equalization for both modulation schemes at the same data rate of 8.9667 Mbps. It is obvious that QPSK outperforms 16-QAM on the behalf of having double the number of subcarriers per user which leads to better frequency diversity collection. Another reason supporting 16-QAM's poor performance, is the tighter decision boundaries which leads to more error events. It can be noted that there is around 6 dB degradation with 16-QAM modulation at high SNRs.

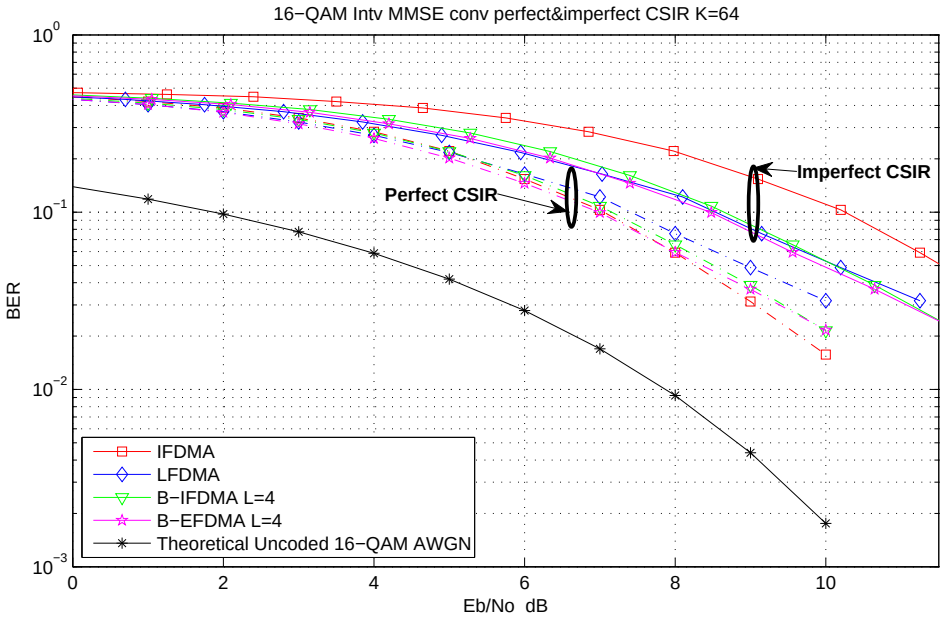

Figure 5.13. 16-QAM with MMSE, Convolutional Coding, Interleaver under Perfect and Imperfect Channel Knowledge.

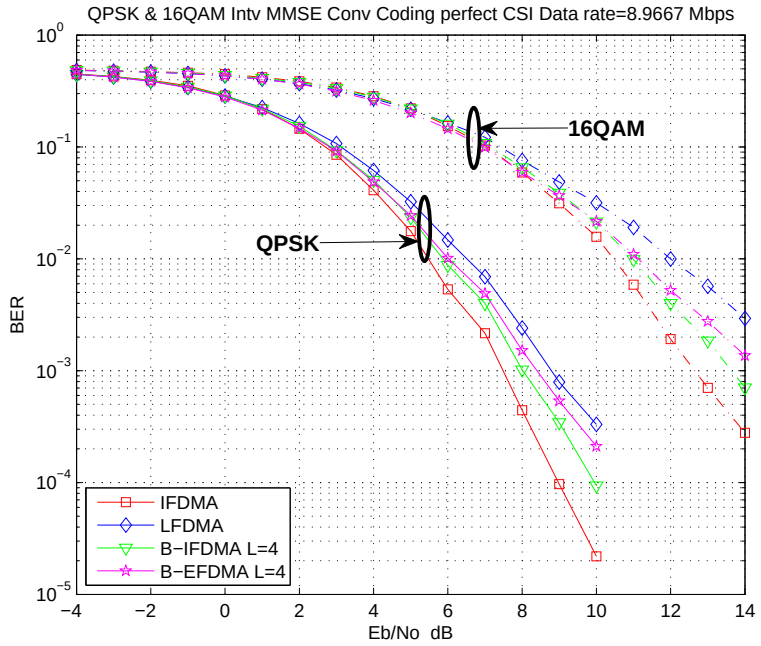

Figure 5.14. QPSK and 16-QAM with MMSE, Convolutional Coding, Interleaver under Perfect CSIR.

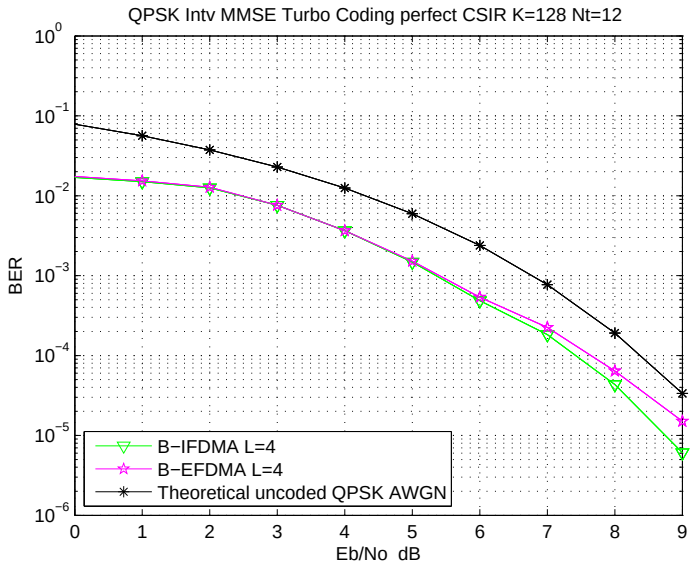

Figure 5.15. QPSK with MMSE, Turbo coding, Interleaver under Perfect CSIR.

Simulations with Turbo Codes

The same system with MMSE and interleaving was simulated with the deployment of Turbo codes implemented by (Wu 1998) and the two modulation schemes QPSK and 16-QAM. Figure 5.15 shows the BER performances of B-IFDMA and B-EFDMA with 4 subcarriers per block. The DFT-precoded B-IFDMA beats the non DFT-precoded B-EFDMA after an SNR of 6 dB, while the two were overlapping before that. It should be noted that Turbo codes were able to collect the diversity provided by both schemes.

Figure 5.16 shows the BER performances while using 16-QAM. In this case, both schemes were behaving almost in a similar fashion until an SNR of 8 dB, where B-IFDMA takes the lead in delivering a slightly better performance.

A nice comparison will be to see the performance of the system with QPSK and 16-QAM to highlight the negative effect of higher order tighter constellation on the performance as shown in figure 5.17.

Finally, to see the effect of collecting frequency diversity on the BER performances, some investigations were done by varying the block size of B-EFDMA and B-IFDMA as shown in figure 5.18. The performance of both schemes was the same until an SNR of 5 dB, after which B-IFDMA provided a slightly better performance.

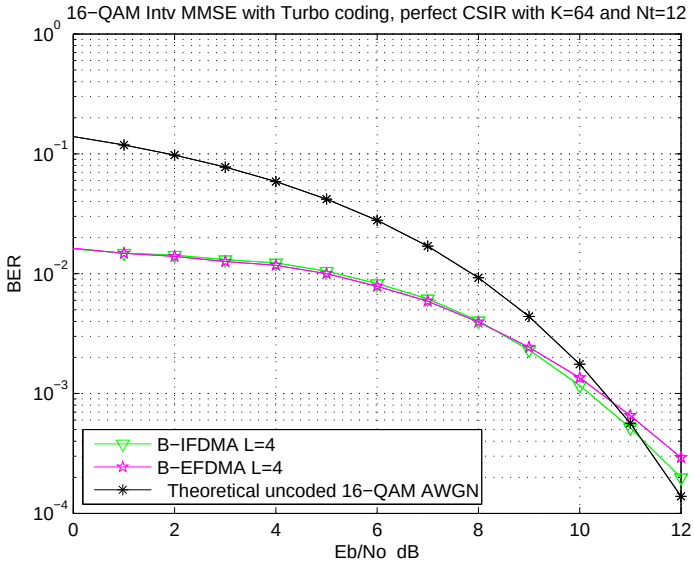

Figure 5.16. 16-QAM with MMSE, Turbo Coding, Interleaver under Perfect CSIR.

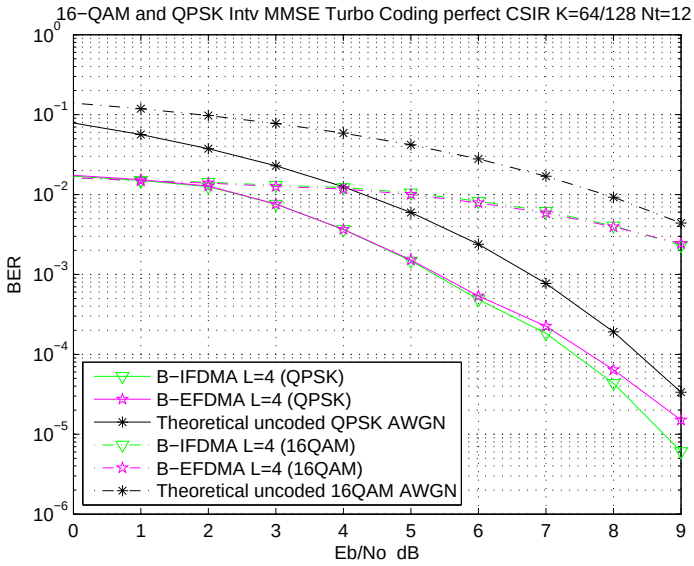

Figure 5.17. QPSK and 16-QAM with MMSE, Turbo Coding, Interleaver under Perfect CSIR.

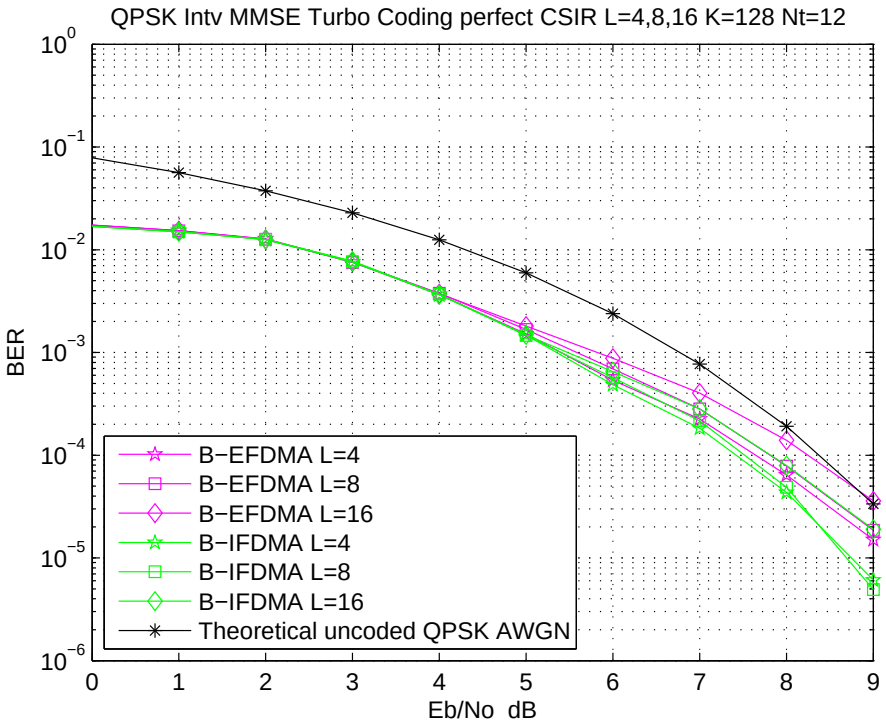

Figure 5.18. QPSK with MMSE, Turbo coding, Interleaver under Perfect CSIR with Varying Block Size.

6 CONCLUSION AND FUTURE WORK

The essence of this thesis highlights the trade-off between frequency diversity, PAPR, and channel estimation(Perfect, Imperfect) at the receiver, in the presence of different equalizers (ZF, MMSE), channel codes (Convolutional, Turbo), for different modulation (QPSK,16-QAM) schemes for the uplink multiple access (DFT-precoded, Non DFT-precoded) intended for IMT-Advanced.

The trade-off for systems with convolution codes, could be summarized by the following:

Zero Forcing Equalization

- Non DFT-precoding schemes provides a better BER performance.
- For QPSK, decreasing the block size leads to a better performance after an SNR of 7 dB for the non DFT-precoded case, and after an SNR of 10 dB for the DFT-precoded case. Whereas for 16-QAM the same trend should be noticed but at much higher SNRs.
- For QPSK, interleaving is good for non-DFT precoding schemes and for an SNR $\geq$ 6 dB. Same thing holds for 16-QAM, but after an SNR of 12 dB. It should be noted that non DFT-precoded systems gains more from interleaving at the simulated SNRs. DFT-precoded schemes should also gain from interleaving but at much higher SNRs.
- Interleaver depth has no significant effect on the performance.

MMSE Equalization

- For QPSK, DFT-precoded systems performs better after an SNR of 2 dB, whereas 16-QAM, the same conclusion holds but after an SNR of 7 dB.
- Decreasing the block size leads to better performance for QPSK. Whereas for 16-QAM, the trend is similar but after an SNR of 7 dB.
- Interleaving is important for both modulation schemes, and QPSK gains from it after an SNR of 3 dB while 16-QAM, after an SNR of 8 dB. It should also be noted that non DFT-precoded systems gain more from interleaving.
- Interleaver depth has no significant effect on the performance.
- In the case of imperfect CSIR with an interleaver, LFDMA approaches B-IFDMA and B-EFDMA for QPSK up till an SNR of 6 dB. After that, diversity collecting schemes start to perform better. For 16-QAM, same conclusion

holds but B-EFDMA approaches B-IFDMA. Like in QPSK, frequency diversity collecting schemes should perform better at much higher SNRs.

Although turbo channel codes provide an excellent BER performance for moderate SNRs, collecting the diversity provided by these mapping schemes still has an effect on performance. Decreasing the block size leads to a better BER performance.

Future Work

The results of this work could be extended to a couple of future research directions. The areas of interest that we foresee as of valuable impact are related to deeper analysis of the effect of more robust equalization schemes, e.g. Turbo Equalizers. Also it would be interesting to see the effect of Adjacent Channel Interference, thus allowing more work to be done on stronger algorithms to compensate it.

Appendix A

SIMULATION OF RAYLEIGH FADING CHANNEL

In this Appendix the simulation of a time frequency varying Rayleigh fading channel using Jake's or Clarke's doppler spectrum is explained.

There are two popular methods to simulate Rayleigh fading (Ström and Seifi 2008), first is filter method based on the autocorrelation property and the second is spectrum method based on the power spectral density of the fading random process. We will concentrate on the spectrum method since it is efficient and faster compared to the filter method.

A.1 Spectrum Method

The idea behind the spectrum method is to obtain time samples of the Rayleigh fading by transforming the samples of the fading gain in frequency domain using inverse fourier transform. Where $T_s = 1/f_s$ is the sampling period and should be chosen to have no aliasing effect. We know for Clarke's model the power spectral density $S_c(f)$ is defined as

$$S_c(f) = \begin{cases} \frac{1}{\pi f_D} \frac{1}{\sqrt{1-(f/f_D)^2}}, |f| \leq f_D \\ 0 \, otherwise. \end{cases}$$

Obtain $\tilde{G}(f)$ as $G(f) + G(f - f_s)$ shown in figure A.1, where $G(f)$ is the square root of power spectral density. Now the time domain fading samples $c(nT_s)$ are generated by taking N_s-point IFFT on $\tilde{G}(kf_s/N_s)Z(k)$. $Z(k)$ is the complex Gaussian random processes with zero mean and variance of $Z(k)$ is chosen so that generated time domain fading samples to have unit variance.

A.2 Time-Frequency Varying Channel

The discrete time model for time frequency varying Rayleigh fading channel is shown in figure A.2. It is modeled as tapped delay line filter where each tap has some

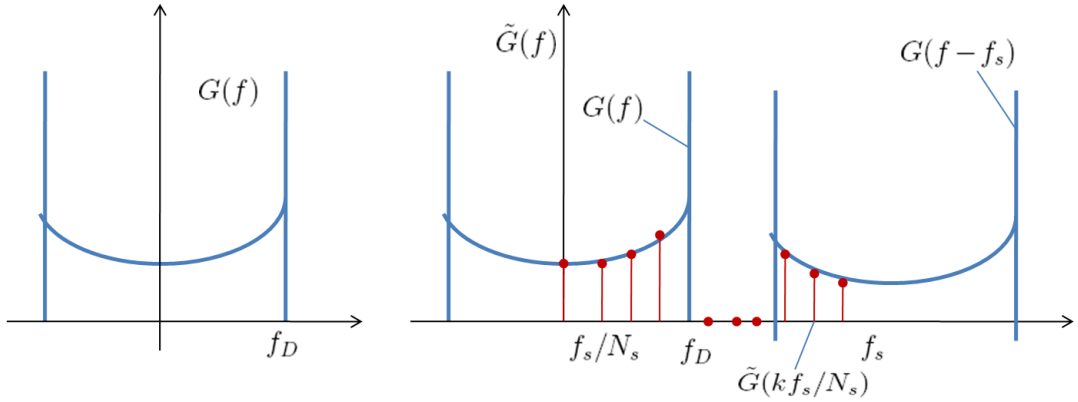

Figure A.1. $\tilde{G}(f)$ and its Samples $\tilde{G}(kf_s/N_s)$ for $N_s = 10$ and $k = 0, 1, \ldots, N_s - 1$.

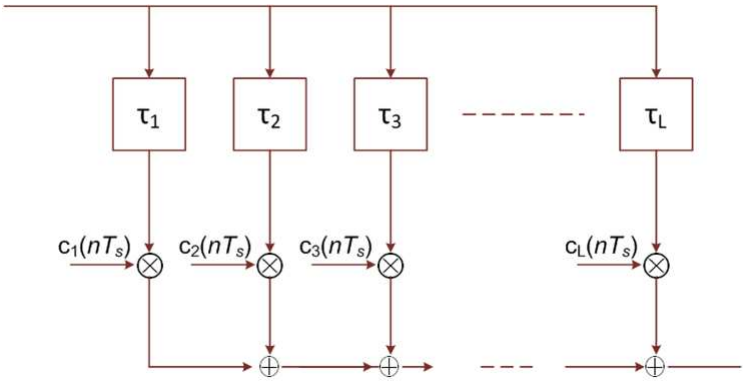

Figure A.2. Discrete Time Model of Time Frequency Varying Channel.

complex gain and delay. This models the practical channel with different multipath components in which each component contributes some delay and attenuation to the transmitted signal. L corresponds to number of resolvable multipath components in figure A.2.

The time and frequency varying channel response $C(f, nT_s)$ can be written as

$$C(f, nT_s) = \sum_{l=1}^{L} c_l(nT_s) exp(-j2\pi f \tau_l T_s.) \tag{A.1}$$

Now sampling the time varying frequency response at frequencies $f = k/(NT_s)$ for $k = 0, 1, 2, \ldots, N-1$ we get

$$\begin{aligned} C(\frac{k}{NT_s}, nT_s) &= \sum_{l=1}^{L} c_l(nT_s) exp(-j2\pi \frac{k}{NT_s} \tau_l T_s) = \sum_{l=1}^{L} c_l(nT_s) exp(-j2\pi \frac{k}{N} \tau_l) \\ &\triangleq C[k, n]. \end{aligned}$$

The time frequency varying response for 64 subcarriers of the WINNER C2 NLOS channel in which the power delay profile has been normalized to unity is shown in figure A.3.

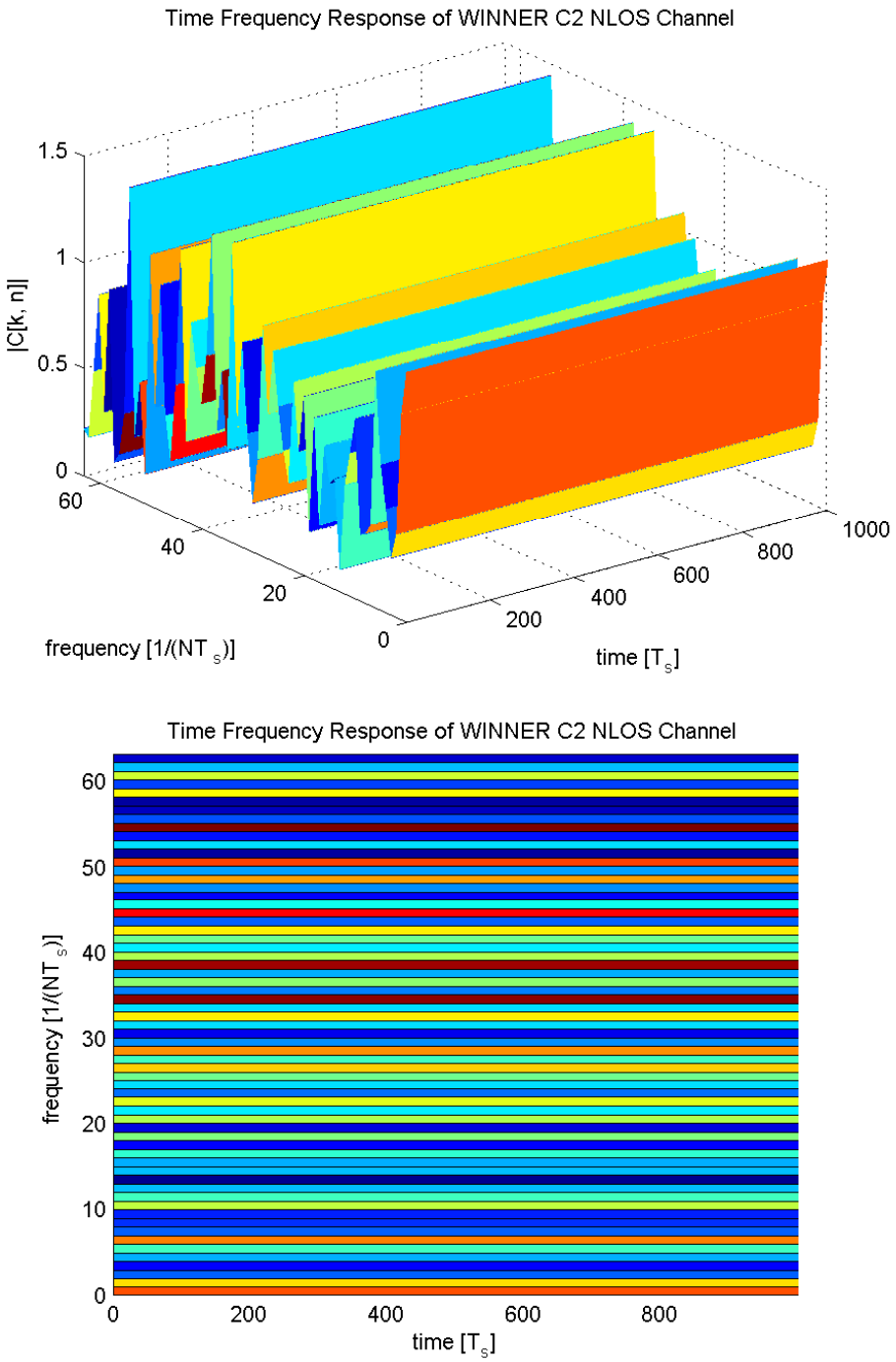

Figure A.3. Time Frequency Varying Response of WINNER C2 NLOS Channel.

Appendix B

ADDITIONAL RESULTS

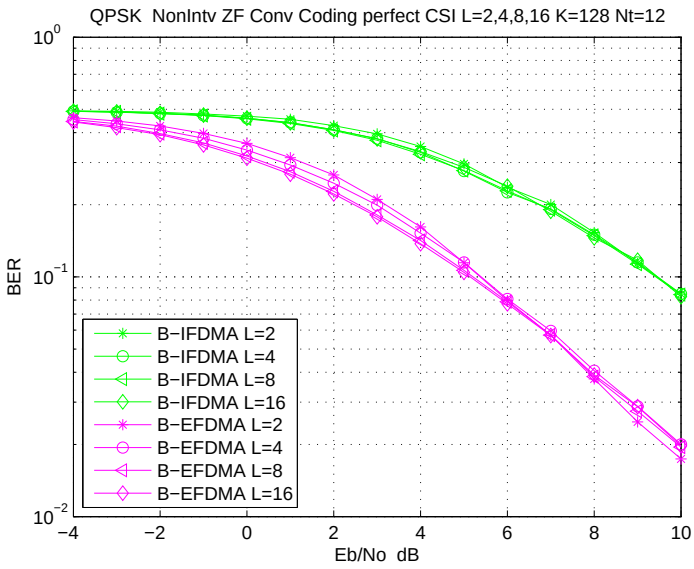

Figure B.1. QPSK NonIntv with ZF, Convolutional Coding and Perfect Channel Knowledge while Varying Block Size.

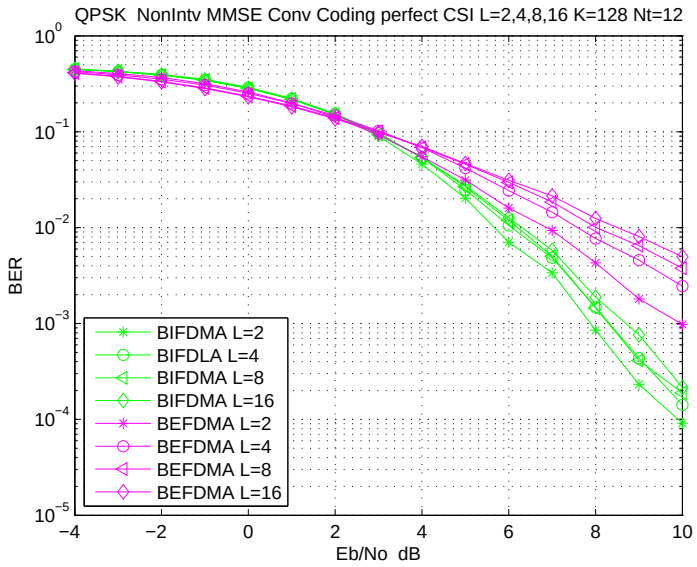

Figure B.2. QPSK NonIntv with MMSE, Convolutional Coding and Perfect Channel Knowledge while Varying the Block Size.

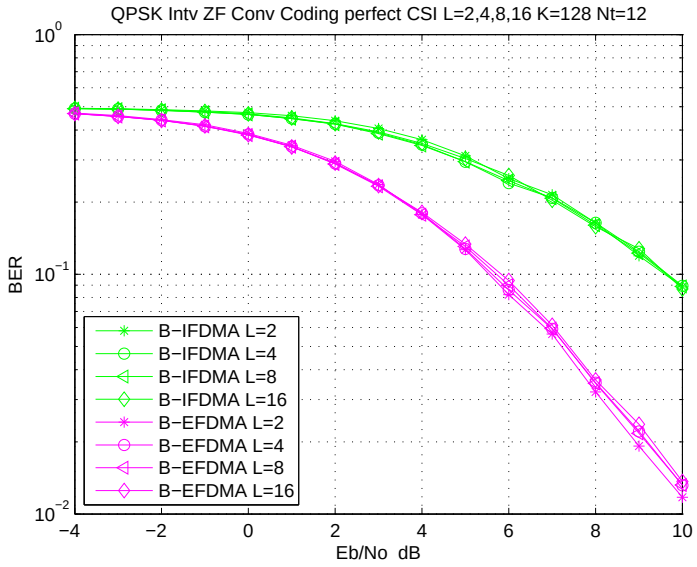

Figure B.3. QPSK Intv with ZF, Convolutional Coding and Perfect Channel Knowledge while Varying the Block Size.

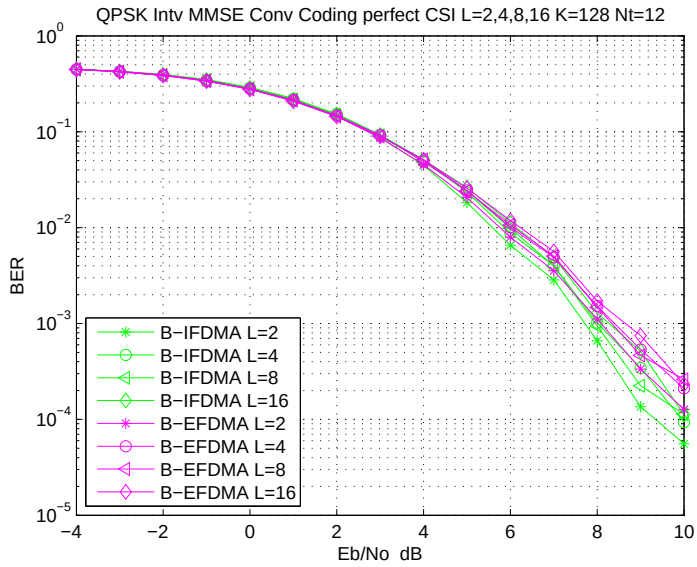

Figure B.4. QPSK Intv with MMSE, Convolutional Coding and Perfect Channel Knowledge while Varying the Block Size.

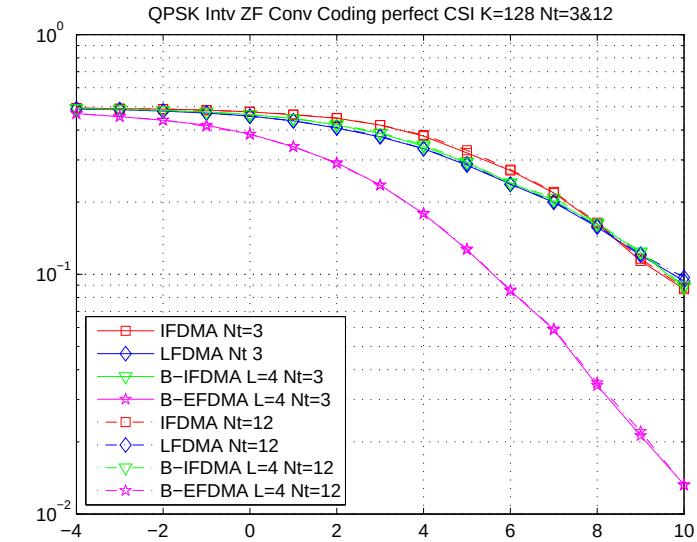

Figure B.5. QPSK Intv with ZF, Convolutional Coding and Perfect Channel Knowledge while Varying the Depth of the Interleaver.

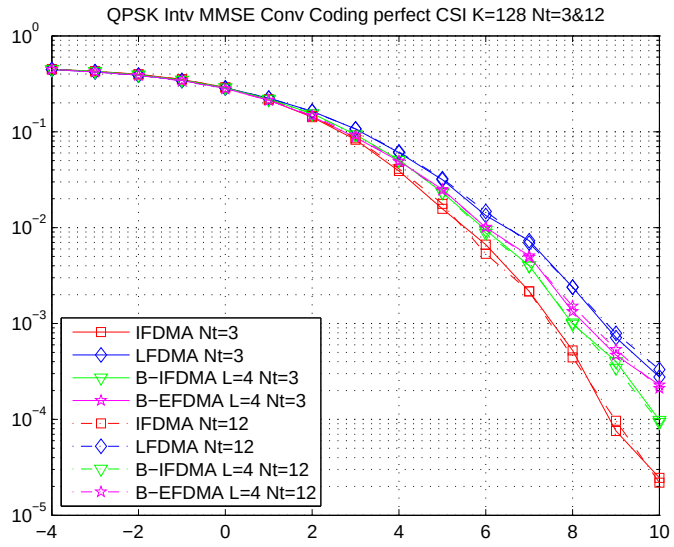

Figure B.6. QPSK Intv with MMSE, Convolutional Coding and Perfect Channel Knowledge while Varying the Depth of the Interleaver.

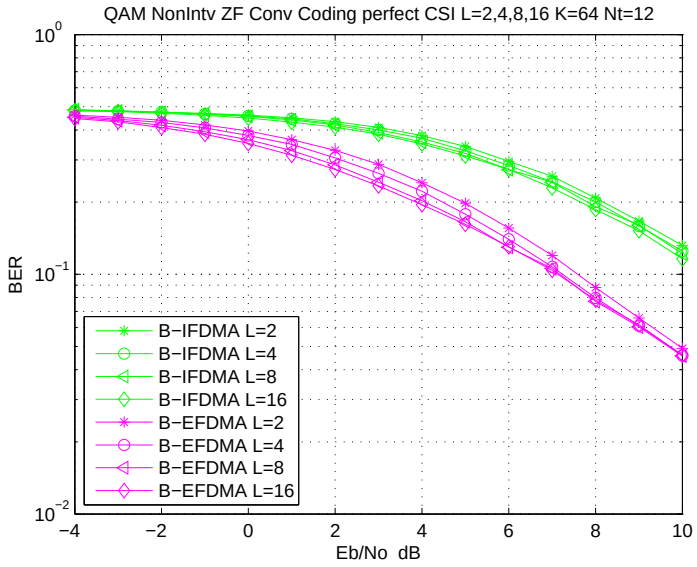

Figure B.7. 16-QAM NonIntv with ZF, Convolutional Coding and Perfect Channel Knowledge while Varying the Block Size.

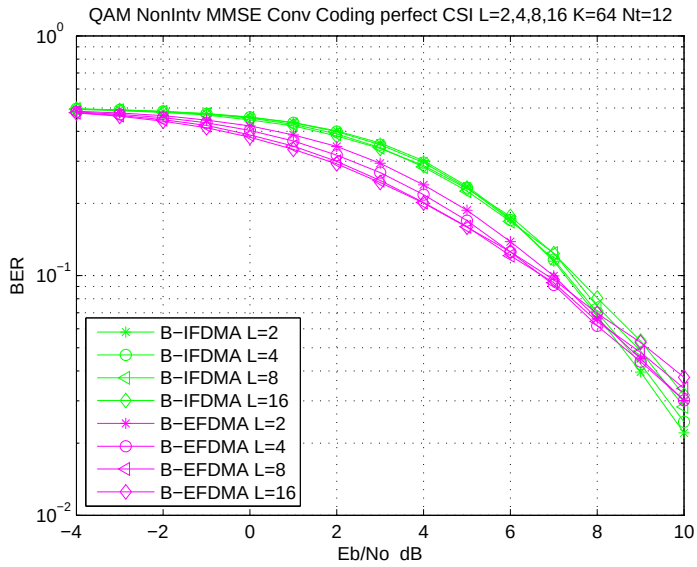

Figure B.8. 16-QAM NonIntv with MMSE, Convolutional Coding and Perfect Channel Knowledge while Varying the Block Size.

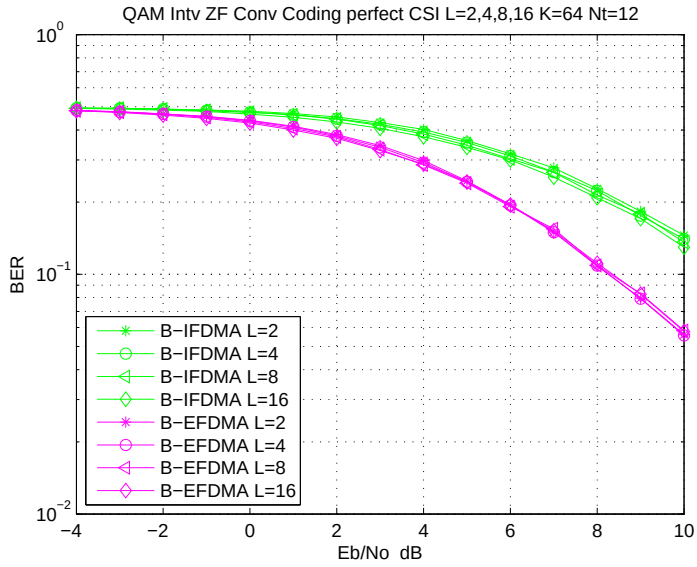

Figure B.9. 16-QAM Intv with ZF, Convolutional Coding and Perfect Channel Knowledge while Varying the Block Size.

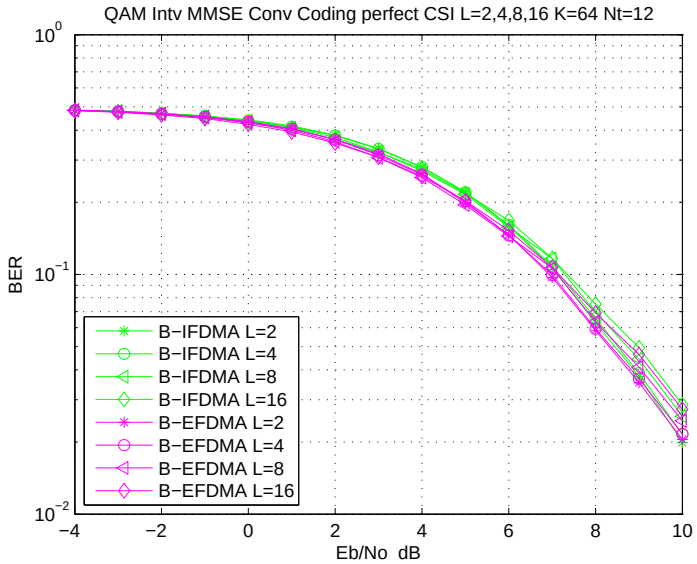

Figure B.10. 16-QAM Intv with MMSE, Convolutional Coding and Perfect Channel Knowledge while Varying the Block Size.

Bibliography

Aronsson, D., Svensson, T. and Sternad, M. (2009). Performance evaluation of memory-less and Kalman-based channel estimation for OFDMA. In: *Proc. IEEE Vehicular Technology Conference VTC09-Spring*. Barcelona, Spain. To appear, available on http://www.signal.uu.se/Publications/wip.html.

Baum, D., El-Sallabi, H. et al. (Nov. 2005). D5.4 v1.4 final report on link level and system level channel models. *IST-2003-507581 WINNER*.

E. Dahlman, S. Parkvall, J. Skold P. Beming (2008). *3G Evolution: HSPA and LTE for Mobile Broadband*. Academic Press Inc.

Gentile, K. (2007). Digital pulse-shaping filter basics. Technical report. Analog Devices.

Goldsmith, Andrea (2005). *Wireless communications*. Cambridge University Press. Cambridge ; New York.

Lie Qian, Yiyan Tang, Yuke Wang M.O. Ahmad M.N.S Swamy (n.d.). Explore parallelism for viterbi decoder implementation on dsp. Technical report. University of Texas at Dallas and Concordia University.

Myung, H.G., Lim, J. and Goodman, D. J. (2006). Single carrier FDMA for uplink wireless transmission. *IEEE Vehicular Technology Magazine*, **1**, 30–38.

Myung, Hyung G. and Goodman, David J. (2008). *Single carrier FDMA : a new air interface for long term evolution*. Wiley series on wireless communications and mobile computing. J. Wiley & Sons. Chichester, U.K. ; New York.

Pål Frenger, Pål Orten and Ottosson, Tony (1999). Convolutional codes with optimum distance spectrum. *IEEE Communications Letters*, **3**(11), 317–319.

Rappaport, Theodore S. (2002). *Wireless Communications: Principles and Practice,2nd Edition*. Prentice Hall Communications Engineering and Emerging Technologies Series.

Rodger E. Ziemer, Roger L. Peterson (Aug 2000). *Introduction to Digital Communication, 2nd Edition*. Prentice Hall Publications.

Rumney, M. (2008). Introducing single-carrier fdma. Technical report. Agilent Technologies.

Sadeghi, Parastoo (2006). Lecture notes. Technical report. The Australian National University. Modern Wireless Communication SystemsCourse.

Shu Lin, Daniel J. Costello (2004). *Error Control Coding,2nd Edition*. Prentice Hall Publications.

Sklar, Bernard (1997). Rayleigh fading channels in mobile digital communication systems part i: Characterization. *IEEE Communications Magazine*.

Ström, Erik (2008). Lecture notes. Technical report. Chalmers University. Wireless Communication Course.

Ström, Erik and Seifi, Nima (2008). Simulation of fading wireless channel. Technical report. Chalmers University. Project 1, Wireless Communication Course.

Svensson, T., Frank, T. et al. (2007). B-IFDMA - a power efficient multiple access scheme for non-frequency-adaptive transmission. In: *Mobile & Wireless Communications Summit*. Budapest, Hungary.

The 3rd Generation Partnership Project (3GPP) (2006). Physical layer aspects for evolved Universal Terrestrial Radio Access (UTRA). Technical Report TR 25.814 v7.1.0.

V. Pereira, T. Sousa (2004). Evolution of mobile communications: from 1g to 4g. Technical report. University of Coimbra.

Woerner, B. D (1994). Lecture notes. Technical report. Virginia Tech. EE 5984 - Digital Communications.

Wu, Yufei (1998). Turbo code implementation. Technical report. Virginia Tech .